

Destabilization of buried carbon under changing moisture regimes

Manisha Dolui^{1†}, Teneille Nel^{1*†}, Abbygail R. McMurtry²,
Stephanie Chacon¹, Joseph A. Mason³, Laura M. Phillips²,
Erika Marin-Spiotta³, Marie-Anne de Graaff²,
Asmeret Asefaw Berhe¹, Teamrat A. Ghezzehei¹

¹*Department of Life and Environmental Sciences, University of
California, Merced, 5200 Lake Rd, Merced, California, 95343, United
States.

²Department of Geography, University of Wisconsin-Madison, 550
North Park Street, Madison, Wisconsin, 53706, United States.

³Department of Biological Sciences, Boise State University, 1910
University Drive, Boise, Idaho, 83725, United States.

*Corresponding author(s). E-mail(s): teneille.nel@gmail.com;

†These authors contributed equally to this work.

Abstract

Paleosols formed by the burial of topsoil during landscape evolution can sequester substantial amounts of soil organic carbon (SOC) over millennia due to protection from surface disturbances. We investigated the moisture sensitivity of buried SOC storage in the Brady paleosol, a loess-derived soil in Nebraska, USA, where historical aeolian deposition during the Pleistocene–Holocene transition buried soils up to 6 m deep. Topsoils from erosional (up to 1.8 m depth) and **burial** (up to 5.8 m depth) transects were incubated under two moisture regimes - continuous wetting (60% water-holding capacity) and repeated drying–rewetting - to assess soil organic matter (SOM) vulnerability to changing hydrologic conditions. SOC decomposition rates modeled from CO₂ fluxes were consistently higher in erosional than **burial** settings, with surface re-exposure of Brady soils enhancing microbial accessibility and destabilization. A two-pool model showed that >96% of SOC was stored in a slow-cycling pool, particularly in deeply buried soils where stabilization was linked to mineral association, fine particles, and Ca-mediated flocculation. However, this pool decomposed more rapidly in **shallower Brady**

001
002
003
004
005
006
007
008
009
010
011
012
013
014
015
016
017
018
019
020
021
022
023
024
025
026
027
028
029
030
031
032
033
034
035
036
037
038
039
040
041
042
043
044
045
046

047 soils (higher turnover rate relative to buried soil), reflecting increased microbial
048 responsiveness to surface-driven processes.
049 Drying–rewetting cycles caused greater C losses from Brady soils than continuous
050 wetting, despite the dominance of the slow pool and depletion of labile C. These
051 cycles also accelerated fast pool decay in modern soils and erosional transects,
052 whereas burial dampened variability in Brady soils. Although continuous wetting
053 increased overall decay in burial transects during the incubation period, wet–dry
054 cycles destabilized the slow pool, which may result in greater long-term C loss.
055 Together, these results underscore the importance of burial depth, geomorphic
056 context, and moisture regime in shaping the long-term vulnerability of ancient
057 SOC under climate change.

058 **Keywords:** paleosol, erosion, soil carbon stabilization, organic matter decomposition

059

060

061

062 1 Introduction

063

064 Global temperatures have risen by 1°C since the industrial era due to anthropogenic
065 CO₂ emissions, confirming human-driven climate change (IPCC 2018). Alongside
066 warming, precipitation regimes are shifting - marked by increased frequency and
067 intensity of wetting and drying events, especially in more arid ecosystems. These
068 hydrologic fluctuations can destabilize long-stored soil organic carbon (SOC) by
069 disrupting aggregates, increasing dissolution and solute mobility, and stimulating
070 microbial decomposition (Berhe et al. 2012; Min et al. 2020; Hicks Pries et al. 2023).
071 While limiting warming to below 2°C remains critical, mitigation via emissions reduc-
072 tions alone may be insufficient. Preserving or enhancing terrestrial carbon sinks,
073 especially soils, offers a complementary pathway for climate stabilization.

074 Soil organic matter (SOM) encompasses the full suite of organic compounds in soil,
075 including living biomass, particulate debris, and mineral-associated organic molecules.
076 SOC refers specifically to the carbon fraction of SOM and is the metric used through-
077 out this study to quantify carbon stocks and fluxes. While many studies examine
078 topsoil carbon dynamics, whole-soil responses to changes in climate have rarely been
079 tested (Hicks Pries et al. 2017). Subsoils hold nearly half of global SOC stocks (Job-
080 bagy and Jackson 2000) and this deep-soil carbon may be more sensitive to varying
081 environmental conditions than surface soil (Min et al. 2020). Organic inputs reach
082 subsoils via leaching of dissolved organic carbon and vertical transport of litter by
083 bioturbation. SOC in deeper horizons typically features low carbon to nitrogen (C:N)
084 ratios and long mean residence times, suggesting advanced microbial processing and
085 relative stability (Rumpel and Kögel-Knabner 2011). In contrast, topsoils buried by
086 aeolian or alluvial deposition often retain legacy carbon signatures reflecting past veg-
087 etation and climate (Marin-Spiotta et al. 2014), diverging from modern surface soils.
088 These buried soils have historically been isolated from near-surface conditions, includ-
089 ing temperature and moisture fluctuations. Previous research supports this isolation
090 effect: for instance, Chaopricha (2013) found negligible CO₂ fluxes from Brady Soil
091 collected from 4 m below the modern surface when no water was added, indicating
092 extremely limited microbial activity under such dry, oxygen-poor conditions.

The stability of buried SOC, however, depends entirely on continued isolation from surface conditions – an assumption increasingly at odds with landscape dynamics across the Great Plains. Accelerated gully erosion, agricultural tillage, and more intense precipitation events are progressively exhuming paleosols that remained protected for millennia (Mason et al. 2008; Jacobs and Mason 2007; Thaler et al. 2021). Yet the decomposition response of this ancient carbon to re-exposure remains poorly constrained. Will millennia-old SOC decompose rapidly once oxygen and moisture access is restored, or do the same properties that enabled its long-term preservation – fine texture, mineral associations, chemical recalcitrance – confer lasting resistance? This uncertainty carries substantial implications for carbon-climate feedbacks: if re-exposed paleosol carbon proves vulnerable to decomposition, ongoing erosion across loess landscapes could convert a long-term carbon sink into an unaccounted source.

Subsurface environments typically have limited oxygen, C inputs, and water availability, all of which constrain microbial activity and promote long-term SOC persistence (Soong et al. 2021). However, this protection may be compromised under climate change scenarios involving increased rainfall, warming, and surface disturbance (Fontaine et al. 2007; Gao et al. 2020; Hicks Pries et al. 2023). While burial isolates SOM from decomposers, enhancing its stability (Berhe et al. 2007; Stacy et al. 2015; Berhe et al. 2008), soil erosion, root intrusion, and hydrologic shifts can re-expose previously protected SOM. While erosion may remove C, the exposure of fresh relatively unweathered parent material can increase photosynthate additions due to the rejuvenation of rock-derived nutrients (Berhe et al. 2018). Given the global extent of geomorphic disturbance and the potential for reactivated decomposition, buried soils may represent an extensive but under-characterized carbon pool whose long-term persistence is uncertain (Chaopricha and Marín-Spiotta 2014; Szymanski 2021; Pal et al. 2023).

SOM decomposition is mediated by geomorphic and geochemical controls. Soil texture, mineralogy, and ionic composition regulate organo-mineral associations and microbial accessibility. Mineral surfaces – particularly clays and metal oxides – can stabilize SOM through sorption and aggregation, while spatial inaccessibility and microsite heterogeneity further constrain decomposition (Marin-Spiotta et al. 2011; Schmidt et al. 2011; Lawrence et al. 2015). Thermal transformation of buried SOM into condensed aromatic compounds can also enhance resistance to decay. Recent findings from Dolui et al. (2026b) link persistent SOM turnover in buried soils to fine textures, higher conductivity, and strengthened organo-mineral bonding, consistent with evidence that mineral-associated and physically protected pools dominate long-term persistence (Slessarev et al. 2022). However, these stabilizing mechanisms weaken with erosional exposure, as disruption of aggregates, increased oxygen availability, and shifts in moisture regimes enhance microbial activity. In addition, exposure promotes priming effects through fresh organic matter inputs, accelerating the decomposition of previously protected SOM (McMurtry et al. 2024; Lawrence et al. 2021) and increasing its vulnerability to loss.

Soil moisture dynamics are central to SOM persistence. Wetting and drying–rewetting cycles can destabilize aggregates, increase dissolved organic carbon leaching, and stimulate mineral-associated OM loss (Berhe et al. 2012; Neff and Asner

139 2001; Li et al. 2023). Moisture influences microbial processes by modulating water
140 potential, oxygen diffusion, and solute transport (Chowdhury et al. 2011; Davidson
141 et al. 2012). Texture controls water retention during drying, while aggregate structure
142 governs accessibility under saturated conditions (Or and Tuller 1999; Ghezzehei et al.
143 2019).

144 In surface soils, especially in semi-arid and Mediterranean systems, dry-
145 ing–rewetting cycles produce strong mineralization pulses (Miller et al. 2005; Zhu and
146 Cheng 2013). Such cycles break down aggregates and release labile SOM, stimulating
147 priming effects (Najera et al. 2020). Soils with broader pore-size distributions may
148 retain water longer, sustaining microbial activity and potentially increasing cumula-
149 tive SOM loss (Goebel et al. 2005). The effects of increased rainfall also depend on
150 seasonal timing; for instance, winter precipitation can enhance subsoil C storage more
151 than spring rain due to deeper translocation of carbon (Wahab et al. 2025).

152 As soils dry, physical and chemical processes can strengthen OM–mineral interac-
153 tions. Solute precipitation, matric tension, and shifts toward stronger bonding (e.g.,
154 inner-sphere complexes) promote greater SOM–mineral affinity (Kaiser et al. 2015;
155 Kemper et al. 1987; Kang and Xing 2008). Reorientation of amphiphilic compounds on
156 mineral surfaces can increase hydrophobicity (Horne and McIntosh 2000), potentially
157 misleading assessments of SOM stability under drier conditions.

158 CO₂ efflux in subsoils is shaped by physical constraints - lower porosity, higher
159 bulk density, and greater water-filled pore space - which suppress microbial respiration
160 after rewetting (Min et al. 2020; Hill et al. 1985; Beare et al. 2009; Schrumpf et al.
161 2013). Subsurface microbial communities are often dominated by drought-tolerant
162 fungi (Bird and Torn 2006), and experience fewer moisture and temperature fluctua-
163 tions than surface soils (Rumpel and Kögel-Knabner 2011). Microbial “resistance” to
164 drying manifests as reduced respiration during dry-down, while “resilience” describes
165 rapid respiration rebound after rewetting (Leizeaga et al. 2021; Griffiths and Philip-
166 pot 2013). Soils with frequent drying–rewetting history tend to support more resilient
167 microbial communities (Fierer and Schimel 2003; Steenwerth et al. 2005).

168 In semi-arid systems, soil inorganic carbon (SIC) also contributes to carbon dynam-
169 ics. SIC accumulates at depth through carbonate dissolution–precipitation cycles
170 (Shariffar et al. 2023; Batool et al. 2024; Cotrufo and Lavallee 2025). This is seen in
171 the Brady Soil, a late Pleistocene paleosol buried by loess ca. 13,000–10,000 years ago
172 in the Great Plains of the US (Jacobs and Mason 2007; McDowell 2020). SIC inter-
173 acts with SOC via aggregation and mineral associations but can be mobilized through
174 leaching under increased moisture conditions (Naorem et al. 2022; Liu et al. 2018;
175 Tsy-pin and Macpherson 2012).

176 Despite growing interest in buried SOM, moisture-driven decomposition patterns
177 across landforms remain unclear. This study investigates the sensitivity of modern
178 and buried SOM to moisture inputs under erosional and burial geomorphic conditions
179 in the Brady Soil. According to the U.S. National Climate Assessment (2018), the
180 Central Great Plains region of Nebraska is projected to warm by 3.5–9.5°C, with
181 annual precipitation increasing by 2.5 cm. Erosion driven by agriculture, grazing,
182 wind, and rainfall threatens to re-expose buried SOM to surface conditions.

183
184

We conducted a laboratory incubation using soils collected near Wauneta, Nebraska, to compare CO₂ efflux under continuous wetting versus drying–rewetting regimes. The area’s semi-arid climate with seasonal moisture variability provides a relevant setting to test SOM responses to hydrologic fluctuations. Our hypotheses were: (i) Brady SOM is more stable and decomposes more slowly than modern SOM as reduced moisture and oxygen availability limit decomposition of SOM due to isolation from the soil surface; (ii) buried SOM in erosional settings is more vulnerable to loss due to exposure of previously protected SOM to surface conditions and mixing with modern carbon; and (iii) wetting will stimulate CO₂ release from previously buried soils as a result of increased substrate availability due to enhanced dissolution, solute transport, microbial decomposition, and/or aggregate disruption. By evaluating the interactions between moisture, geomorphology, and SOM dynamics, we aim to improve predictions of carbon stability under future climate and land-use change.

2 Methods and materials

2.1 Site and sampling

The field site is situated near Wauneta, within the loess tablelands of southeastern Nebraska, USA (40°29’52.8” N, 101°24’36” W; see Fig. 1). The region experienced reduced loess input during the terminal Pleistocene and early Holocene (13–10 ka) that permitted soil formation, leading to the development of the Brady Soil. Subsequent aridification renewed dust flux, resulting in its burial by younger loess (Johnson et al. 2007; Mason et al. 2008). Additional loess accumulation throughout the Holocene preserved weaker paleosols formed during intermittent burial pauses (Mason et al. 2003; Miao et al. 2007). Recognized as a key paleoenvironmental and stratigraphic unit, the Brady Soil is regionally traceable across Nebraska, northeastern Colorado, and northern Kansas (Johnson and Willey 2000).

The area is characterized by broad, flat uplands and sharply incised edges, providing natural windows into stratified soil profiles. Loess cover above the Brady Soil tapers in a downwind direction across the summits where it is thickest, producing burial transects of variable thickness. The local climate is semi-arid, with an average annual temperature of 9.7°C and ca. 495 mm of precipitation, concentrated during the summer months, with occasional snow in winter. Natural vegetation includes a mix of C3 and C4 grasses, replaced by cropland on many level surfaces today, but remaining at the study site and on steeper terrain in general.

Brady Soil exposures are visible in actively eroding margins, gullies, and roadside cuts. Prior investigations, including coring and field surveys, confirm its continuity beneath the summit landform (Jacobs and Mason 2004; Marin-Spiotta et al. 2014; Mason et al. 2008). Surface soils developed in Holocene loess are weakly developed and light-colored, typically classified as Mollisols, Inceptisols, or Entisols. Although different in age, modern and buried soils share similar parent material and mineralogy due to the region’s limited weathering intensity. Brady A horizons (Ab) are identified by their dark grayish brown coloration (Munsell 10YR3/2 to 10YR4/2) and silt loam texture, generally overlying Bk or Bw horizons (Szymanski 2021; Jacobs and Mason 2007; McDowell 2020).

231 Sampling was conducted in 2016 and 2017 across two geomorphic settings: burial
232 transects (where the Brady Soil is deeply buried beneath Holocene loess) and erosional
233 transects (where the Brady Soil is exposed or shallowly buried due to hillslope erosion).
234 Within each setting, three replicate transects were established. We collected samples
235 at three depths relative to the soil surface from each of the transects per setting
236 (details in Fig. 1). Sampling stratigraphy relative to the present land surface was
237 categorized using Roman numerals (Supplementary Information, Table A1). At each
238 transect position, samples were collected from (1) the modern soil surface (0–30 cm),
239 (2) the subsurface modern soil (30–60 cm, where present), and (3) the upper Brady
240 paleosol horizon (0–30 cm into the Ab horizon, at variable depth below the modern
241 surface depending on burial thickness). All samples were analyzed for physicochemical
242 properties, but only samples from the 0–30 cm depth intervals were used for incubation
243 experiments. Table A1 provides the specific sampling depths from the soil surface for
244 each transect position. A Giddings probe (10.2 or 8.9 cm diameter) with plastic liners
245 was used for intact sampling in burial settings, while soil pits were dug for erosional
246 profiles. Complete methods are described in (Szymanski 2021).

248 2.2 Soil chemical and physical analyses

249 General soil physical and chemical properties were determined by standard soil ana-
250 lytical methods, as described in detail in Dolui et al. (2026b) and Szymanski (2021).
251 Briefly, soil pH and electrical conductivity (EC) of soil samples were determined in
252 1: 2 water extracts using a SevenExcellence multiparameter benchtop meter (Met-
253 tler Toledo, United States). Total carbon was determined by dry combustion using
254 an ECS 4010 elemental combustion analyzer (Costech Analytical Technologies, Inc.,
255 USA); inorganic carbon was removed by acidification with 1M HCl prior to TOC
256 determination. Exchangeable base cations (Ca^{2+} , Mg^{2+} , Na^{+} and K^{+}) were
257 quantified by ICP-OES (Optima 5300 DV Spectrometer, Perkin-Elmer, Germany) fol-
258 lowing ammonium acetate extraction (buffered to pH 7). Sodium adsorption ratio
259 (SAR) was determined by dividing concentration of Na in soil extract by the square
260 root of half of sum of Ca and Mg concentrations (Dolui et al. 2026a). Particle size
261 distribution was determined using the pipette method for clay ($< 2\mu\text{m}$) and laser
262 diffraction (Mastersizer 2000 particle size analyzer, Malvern Panalytical, UK) for silt
263 and sand fractions. Radiocarbon (^{14}C) analyses of bulk soil samples were conducted
264 to determine the age and turnover time of carbon in both modern and buried soils.
265 Samples were pre-treated, combusted, and then measured by accelerator mass spec-
266 trometry using an FN accelerator mass spectrometer (Van de Graaff, US) at the
267 center for accelerator mass spectrometry at Lawrence Livermore National Laboratory.
268 The $\Delta^{14}\text{C}$ results were used in a homogeneous, open-system, steady-state soil carbon
269 decomposition model to estimate carbon turnover times (Dolui et al. 2026b) which
270 were averaged for the three replicate transects.

272 2.3 Incubation experiments

273 The incubation experiment was set up to determine the effect of continuous wetting
274 and drying–rewetting on SOC fluxes using soils that were collected from the upper
275
276

layer of modern and Brady Soil samples at burial and erosional transect types. To isolate the effects of moisture, roots >2 mm were removed by sieving and manual sorting. Samples from 0-30 cm horizon depth from different transect numbers were homogenized (so that they had only unique paleostatus, transect type and burial/ erosional degree). Two types of water addition experiments were conducted: continuous wet and drying–rewetting. Two sub-samples were taken from each composite to perform biological replicates of each incubation experiment, such that there was a total number of 24 individual incubation vessels.

2.3.1 Experimental setup

The incubation experiments were conducted in 8 oz mason jars. Soil water holding capacity (WHC) was pre-determined by tensiometry (using pressure plates with an applied pressure of -33 kPa) and soil moisture content was monitored on a mass-basis by weighing soils weekly during the incubation. The treatments included (i) continuous wet – soils maintained at 60% WHC throughout the experiment and (ii) drying–rewetting cycles – soils were dried, then rewetted to 60% WHC. Treatment durations differed by experimental objective. The continuous wet incubation (225 days) was designed to capture the full trajectory of decomposition, enabling robust fitting of two-pool decay models that partition SOC into fast- and slow-cycling fractions (turnover times on the scale of days and centuries, respectively). The wet-dry treatment (56 days, 8 cycles of 7-day drying followed by rewetting) was designed to assess cumulative effects of repeated moisture pulses over a timeframe comparable to a growing season. For direct comparison between treatments, we modeled CO₂ loss over equivalent 49-day windows and compared decay parameters derived from each treatment’s full duration. Each treatment had two biological replicates (sub-samples derived from a single composite of replicate transects per soil type), and control soils were maintained at 5% WHC.

Previously homogenized soils were sub-sampled and added to jars at an equivalent of 30 ± 0.5 g dry mass. After adding a predetermined amount of ultra-pure water (18.2 MΩ · cm), the jars were kept at room temperature (ca. 25°C), matching the average summer soil temperature (when most precipitation occurs) at the site (UNL Soil Temperature Data). Jars were sealed with lids fitted with rubber septa for headspace gas collection, and silicone gel was applied around the septa to prevent gas leakage.

In the continuous wet experiment, soils were maintained at 60% WHC and sealed until sampling. On average, water loss was 0.01 mL/day, ranging from 0.005 to 0.02 mL/day. Water was added after gas sampling to avoid inducing the Birch effect. After each sampling, lids were left open for one hour to allow CO₂ equilibration with ambient air.

In the drying–rewetting experiment, soils were rewetted every 7 days by slowly adding Milli-Q water to reach 60% WHC. After water addition, jars were sealed, and headspace gas was sampled 6 hours later to capture Birch effect emissions. Soils were then dried to 5% WHC over the course of 2-3 days by removing the lids and incubating at ca. 25°C; respiration was not measured during this period.

323 2.3.2 Sampling schedule and CO₂ analysis

324 In the continuous wet experiment, headspace gas samples for CO₂ analysis were col-
325 lected on days 1, 3, 5, 7, 11, 16, 27, 55, 82, 114, 151, and 225. After each sampling,
326 jar lids were opened for one hour to equilibrate with ambient air.

327 In the drying–rewetting experiment, jars were sealed for 6 hours after water addi-
328 tion, and headspace gas was sampled on days 1, 7, 21, 28, 35, 42, and 49 to evaluate the
329 Birch effect. Control samples were collected on the same days for both experiments.

330 Evolved CO₂ concentrations were analyzed using a Shimadzu 2014 gas chromato-
331 graph (Kyoto, Japan) with a thermal conductivity detector at UC Merced and an
332 LI-830 infrared gas analyzer (IRGA) at Lawrence Livermore National Laboratory
333 (LLNL).
334

335 2.4 Statistical analyses

336 All statistical analyses were performed using CRAN-R 4.5.0 (R Core Team 2025). Soil-
337 respired CO₂ measurements from incubation experiments were averaged across two
338 biological replicates per treatment. Control samples were represented by single mea-
339 surements due to sample constraints. Accordingly, statistical comparisons involving
340 controls were interpreted with caution.
341

342 The concentration of soil-respired CO₂ was expressed as the mass of C respired
343 per unit mass of SOC, calculated as:
344

$$345 \mu\text{g C} - \text{CO}_2 \text{ g soil C}^{-1} = \text{mmol air} * \frac{\mu\text{mmol CO}_2}{\text{mol air}} * \frac{10^{-3} \text{ mol air}}{\text{mmol air}} * \frac{12 \mu\text{g C}}{\mu\text{mol C}} * \frac{1}{\text{g TOC}} \quad (1)$$

346 For the continuously wet incubation, cumulative respiration was calculated by
347 summing CO₂ fluxes over the 225-day experiment. Two-pool first-order decay models
348 were fitted to cumulative respiration data according to:

$$349 C_{\text{CO}_2}(t) = C_0 \left(1 - (f_f e^{-k_f t} + f_s e^{-k_s t}) \right) \quad (2)$$

350 where $C_{\text{CO}_2}(t)$ is the cumulative mass of C (μg) respired by day t , C_0 denotes
351 TOC, f_f and f_s represent the fast- and slow-cycling fractions of SOC (with $f_f + f_s =$
352 1), and k_f and k_s are the corresponding decay rate constants. Models were fitted
353 using non-linear least-squares optimization with the `minpack.lm` package (Elzhov et al.
354 2023).

355 For the wet-dry cycling incubation, cumulative respiration was calculated by sum-
356 ming CO₂ fluxes over wetting periods only, assuming negligible respiration during
357 drying phases (Chaopricha 2013). The effective incubation time (t) was approximated
358 as the cumulative duration of wetting events (2 days over a 49-day experiment).
359 Two-pool decay models were initially fitted following the same approach as for the
360 continuously wet incubation.

361 Preliminary model fits indicated that the fast-cycling pool contributed negligibly to
362 respiration during wet-dry cycling (slow:fast pool ratio $\sim 0.999:0.001$), consistent with
363
364
365
366
367
368

a functionally homogeneous system. Consequently, one-pool first-order decay models were also fitted for both incubation treatments:

$$C_{CO_2}(t) = C_0(1 - e^{-kt}) \quad (3)$$

where k represents the single-pool decomposition rate constant.

The effects of transect type, paleostatus, degree of burial or exposure, and their interactions on SOM decomposition parameters (decay rates and pool sizes) were evaluated using linear mixed-effects models, treating biological replicates as a random effect (controls excluded). These analyses were conducted using the `nlme` (Pinheiro et al. 2024) and `emmeans` (Lenth 2024) packages. Significant differences among factor levels were assessed using pairwise Sidak-adjusted comparisons. For the wet-dry cycling experiment, similar models were applied to analyze day-1 CO₂ pulse responses.

Total CO₂ losses during wet-dry cycling (49 days) were compared to modeled CO₂ losses over an equivalent duration under continuous wetting using linear mixed-effects models with paleostatus, transect type, and degree of burial or exposure as fixed effects and replicate as a random effect. Marginal means and pairwise comparisons were used to contrast incubation treatments. For control samples, paleostatus and transect type were treated as fixed effects and degree of burial or exposure as a random effect. Despite limited replication, the large magnitude of difference between control and treatment fluxes (>45-fold) indicates that moisture addition, rather than incubation artifacts, drove observed respiration patterns.

Mean cumulative CO₂ losses between control and treatment groups were further compared using a Welch test following confirmation of unequal variances via a Bartlett test, implemented in the `stats` package (RStudio Team 2019). Linear mixed-effects models were also used to evaluate the effects of transect type and paleostatus on cumulative CO₂ losses in control samples, with degree of burial or exposure treated as a random effect.

Multiple linear regression (MLR) was used to quantify the influence of soil physicochemical properties (soil pH, EC, TOC and TIC contents, SAR, texture, and exchangeable base cations) on modeled SOM decomposition parameters. For the continuously wet incubation, MLR models were applied to fast- and slow-pool decay rates and slow-pool fraction sizes derived from two-pool models. For the wet-dry cycling incubation, MLR analyses were conducted on decomposition rates derived from one-pool models. Model selection followed stepwise forward and backward procedures, prioritizing parsimony based on Akaike Information Criterion (AIC) values using the `MASS` package (Venables and Ripley 2002). Model coefficients, intercepts, R², and root mean squared error (RMSE) were calculated using the `stats` package. Pairwise Pearson correlation matrices were generated to visualize relationships among soil properties and SOM decomposition parameters using the `stats` and `ggplot2` packages (RStudio Team 2019).

3 Results

3.1 General soil properties

The physicochemical properties of soils used in the incubation experiment are shown in Table 5. The soils were relatively alkaline (pH ranging from 6.89 to 7.77), especially the Brady Soil (pH > 7.6). The clay, silt and sand content placed the soils in the texture class category of silt loam. Total organic carbon was higher in modern soils due to active biomass inputs, while inorganic carbon content was higher in the Brady Soil due to carbonate formation (Dolui et al. 2026b). The Brady soil of the burial transect was classified as saline (mean EC of 5.41 dS m⁻¹) and the CEC of soils was moderately high, ranging from 15.17 - 23.31 cmol_c kg⁻¹ and indicating the presence of higher activity clays. The turnover time of bulk soils as derived from radiocarbon-based models, was much greater in the Brady Soil (8327 - 15 654 years) compared to modern soils (576.4 - 1451 years), confirming the long-term stability of SOM in the paleosol (Dolui et al. 2026b). The mean CN ratio in both Brady and modern soils was relatively low (ca. 10), indicating a sufficient supply of N for plant growth and microbial activity.

3.2 Effects of continuous wetting on soil CO₂ efflux

Cumulative C lost from soils via respiration of CO₂ during the continuously wet incubation are shown in Fig. 2. Raw incubation data and figures of merit of statistical comparative tests are available online at DOI: doi: 10.17632/fjw646gpyf.1.

In the continuous wet soil treatment group, modern soils evolved significantly higher CO₂ (mean of 30.6 mg CO₂-C g C⁻¹) compared to Brady Soil (mean of 15.9 ± 2.39 mg CO₂-C g C⁻¹) after 225 days of incubation (p < 0.01). Soils of the erosional transect type had greater cumulative C loss (mean of 29.3 mg CO₂-C g C⁻¹) compared to the burial transect (mean of 17.3 ± 2.39 mg CO₂-C g C⁻¹, p < 0.01). However, the difference between cumulative C losses of erosional vs burial transect types was not significant at the greatest degree of burial and lowest degree of erosion.

Modern soil in the erosional transect had significantly higher cumulative C losses (mean of 35.9 mg CO₂-C g C⁻¹) than modern soil of the burial transect (mean of 25.3 mg CO₂-C g C⁻¹, p < 0.05). Similarly, Brady Soil of the erosional transect had significantly higher cumulative C losses (mean of 22.6 mg CO₂-C g C⁻¹) compared to the burial transect (mean of 9.28 mg CO₂-C g C⁻¹, p < 0.05).

The Brady soil with an intermediate degree of erosion had higher cumulative CO₂ loss (mean of 33.2 mg CO₂-C g C⁻¹) compared to Brady Soil of the lowest and highest degrees of erosion, while the Brady soil with the greatest degree of burial had the lowest cumulative CO₂ loss (mean of 4.14 mg CO₂-C g C⁻¹, differences not significant). For Brady soil of the burial transect, the magnitude of cumulative CO₂ efflux among different degrees of burial was in the order of I > II > III, whereas in the erosional transect, cumulative CO₂ efflux among different degrees of erosion was II > III > I.

The cumulative CO₂ evolution of 60% WHC continuous wet experiments (mean of 23.3 mg CO₂-C g C⁻¹) was significantly greater than control soils maintained at 5% WHC (mean of 0.478 mg CO₂-C g C⁻¹, p < 0.001). Among the control soils, Brady

Soil of the **burial** transect had significantly greater C losses (mean of 0.561 mg CO₂-C g C⁻¹) compared to modern soils (mean of 0.253 ± 0.0683 mg CO₂-C g C⁻¹, p < 0.05), but C losses in modern and Brady Soil were more similar in the erosional transect (mean of 0.254 and 0.444 mg CO₂-C g C⁻¹ for modern and Brady Soil respectively, n.s.).

Significance of differences in cumulative CO₂ losses among degree of burial/ exposure for control samples could not be tested due to lack of replication, but we report observed differences. Among the **burial** transect control soils, Brady soil **with the lowest degree of burial** produced the greatest cumulative CO₂ loss, while modern soil collected from the intermediate degree of burial soil produced the least cumulative CO₂ loss. Among the erosional transect control soils, the most CO₂ was evolved in the **Brady soils with intermediate erosion**, and the lowest CO₂ was evolved in the modern soil collected from the lowest degree of burial.

3.3 Effect of drying and rewetting on soil CO₂ efflux

Daily C lost from soils via respiration of CO₂ during the dry-rewetting incubation are shown in Fig. A1 and cumulative C losses are shown in Fig. 3. Soil respiration data from the dry-rewetting incubation are available online at DOI: doi: 10.17632/fjw646gpyf.1.

The largest respiration fluxes were produced on the first day, with significantly greater cumulative CO₂ loss from modern soils (mean of 0.920 mg CO₂-C g C⁻¹) compared to Brady Soil (mean of 0.729 ± 0.034 mg CO₂-C g C⁻¹, p < 0.01), but the reverse was observed at the greatest **degree of burial**. Respiration pulses declined over time for all soils. Control soils had a lower day⁻¹ pulse CO₂ (mean of 0.295 mg CO₂-C g C⁻¹) compared to the dry-rewetting treatment (mean of 0.824 mg CO₂-C g C⁻¹, p < 0.001), but there was no significant difference between the cumulative CO₂ loss from control (21.9 mg CO₂-C g C⁻¹) and treatments (17.5 mg CO₂-C g C⁻¹) by the final day of incubation.

After 49 days of incubation under wet-dry cycles, the Brady Soil from both the burial and the erosional transects emitted significantly more cumulative CO₂ (0.0183 g CO₂-C g C⁻¹) than Brady Soil incubated under continuously wet conditions (0.009 ± 0.0005 g CO₂-C g C⁻¹, p < 0.001). However, there was no significant difference between cumulative CO₂ loss in modern soils incubated under wet-dry cycles versus continuous wet conditions.

The order of magnitude of total CO₂ emission after 49 days followed the order erosional modern > erosional Brady > **burial** modern > **burial** Brady. Soils of the erosional transect (mean of 18.3 mg CO₂-C g C⁻¹) had significantly greater cumulative CO₂ loss compared to the **burial** transect (mean of 16.7 ± 0.643 mg CO₂-C g C⁻¹, p < 0.01). Modern soil had significantly greater cumulative CO₂ loss (mean of 16.7 mg CO₂-C g C⁻¹) than Brady Soil (mean of 18.3 ± 0.390 mg CO₂-C g C⁻¹, p < 0.001), but the difference was not significant at the intermediate **degree of erosion**. Modern soil **with the highest degree of erosion** emitted significantly more cumulative CO₂ (19.2 mg CO₂-C g C⁻¹) than **modern soil with the greatest degree of burial** (13.9 mg CO₂-C g C⁻¹, p < 0.05). However, the opposite was observed in Brady Soil, where **that with the greatest degree of burial** emitted more cumulative CO₂ (15.6 mg CO₂-C g C⁻¹) compared to the **soil with the greatest degree of erosion** (20.4 mg CO₂-C g C⁻¹,

507 $p < 0.05$). Among the control soils, although Brady Soil emitted more cumulative
508 CO_2 than modern soil, there was no significant difference. This was likely due to large
509 variation of the depth-pooled samples (in absence of control replicates), as a result of
510 the much larger CO_2 loss from Brady Soil of the erosional transect with the lowest
511 degree of erosion compared to other samples.

513 3.4 Decay rates and fraction sizes of soil organic matter pools

514 The decomposition rate of the slow pool and size of the fast pool under continuous
515 wetting is shown in Fig. 4 and the decomposition rate of SOM (single pool) under
516 wet-dry cycles is shown in Fig. 5. Statistical figures of merit of linear mixed-effects
517 models are available online at DOI : doi: [10.17632/fjw646gpyf.1](https://doi.org/10.17632/fjw646gpyf.1).

518 The slow-cycling SOM pool under continuous wetting decayed ca. 2000 times more
519 slowly than the fast-cycling pool, with a significantly lower mean decay rate in the
520 burial transect ($8.68 \cdot 10^{-6} \text{ day}^{-1}$ i.e., 315 years turnover time, henceforth referred to
521 as TOT) compared to the erosional transect ($1.36 \cdot 10^{-5} \pm 6.82 \cdot 10^{-7} \text{ day}^{-1}$ i.e., 201
522 years TOT, $p < 0.01$). Thus, higher decay rates correspond to faster (shorter) turnover
523 times throughout this section. The mean decay rate of the slow-cycling SOM pool of
524 Brady Soil ($6.86 \cdot 10^{-6} \text{ day}^{-1}$ i.e., 399 years TOT) was significantly lower than that
525 of modern soil ($1.54 \cdot 10^{-5} \text{ day}^{-1} \pm 6.82 \cdot 10^{-7}$, i.e., 178 years TOT, $p < 0.001$). The
526 mean decay rate of the slow-cycling SOM pool of modern soil in the burial transect
527 was significantly greater at the greatest degree of burial ($1.53 \cdot 10^{-5} \text{ day}^{-1}$ i.e., 178
528 years TOT), compared to the lowest degree of burial ($9.97 \cdot 10^{-6} \text{ day}^{-1}$ i.e., 275 years
529 TOT, $p < 0.05$).

530 The mean decay rate of the fast-cycling SOM pool of the erosional transect (0.130
531 day^{-1} i.e., 7.68 days TOT) under continuous wetting was significantly higher (i.e.,
532 faster turnover) than that of the burial transect ($0.126 \pm 0.001 \text{ day}^{-1}$ i.e., 7.96 days
533 TOT, $p < 0.05$). The mean decay rate of the fast-cycling SOM pool of Brady Soil in
534 the erosional transect was significantly greater at the greatest degree of erosion (0.144
535 day^{-1} i.e., 6.96 days TOT) compared to the lowest degree of erosion (0.121 day^{-1} i.e.,
536 8.25 days TOT, $p < 0.01$).

537 The decay rate of SOM (one-pool model) under wet-dry cycles did not differ sig-
538 nificantly among soils of different paleostatus or transect type. In the two-pool model,
539 the decay rate of the slow-cycling SOM pool under wet-dry cycles was significantly
540 higher in the erosional transect (0.007 day^{-1} i.e., 129 days TOT) compared to the
541 burial transect ($0.009 \pm .0002 \text{ day}^{-1}$ i.e., 117 days TOT, $p < 0.05$), indicating faster
542 SOM turnover where decay rates were higher. The decay rate of the fast-cycling SOM
543 pool in the burial transect was significantly higher in modern soil ($8.11 \pm 1.94 \text{ day}^{-1}$
544 i.e., 0.123 days TOT) compared to Brady soil (0.558 day^{-1} i.e., 1.79 days TOT).

545 The slow-cycling pools of both modern and Brady Soil under continuous wetting
546 contained a much greater proportion of total SOC ($> 96\%$) than the fast-cycling
547 pool. The fraction size of the fast-cycling pool relative to the slow-cycling pool under
548 continuous wetting was significantly greater in the erosional transect (0.014) compared
549 to the burial transect (0.012 ± 0.0003 , $p < 0.01$) and significantly greater in modern
550 soils (0.0173) compared to Brady Soil (0.009 ± 0.0003 , $p < 0.001$). The fraction size
551 of the fast and slow pools tended to 0 and 1.0 respectively in all soils under wet-dry
552

cycling, nullifying the statistical comparison results among soils of different paleostatus and transect types.

3.5 Decay rates and fraction sizes of soil organic matter pools in continuous wet versus wet-dry experiment

A summary of SOM decomposition model parameters (one-pool and two-pool) of the continuously wet and wet-dry cycling experiments is shown in Table 2. Statistical figures of merit of linear mixed-effects models are available online at DOI : doi: 10.17632/fjw646gpyf.1.

With the one-pool models, the continuously wet soils had a significantly higher decay rate (0.00865 day^{-1} i.e., 116 days TOT) compared to the wet-dry cycles (0.00714 day^{-1} i.e., 140 days TOT, $p < 0.01$), indicating faster turnover under continuous wetting. In the burial transect, the one-pool decay constant of the continuous wet experiment was significantly higher (0.0103 day^{-1} i.e., 97.4 days TOT) than that of the wet-dry cycling experiment (0.00690 day^{-1} i.e., 145 days TOT, $p < 0.001$). However, there was no significant difference between the decay constant of the continuous wet and wet-dry experiments in erosional transects. These trends were observed in both Brady and modern soils.

Among the control soils with one-pool models, the continuous wet experiment had a significantly higher decay rate (0.0376 day^{-1} i.e., 26.6 days TOT) compared to the wet-dry cycling experiment (0.00146 day^{-1} i.e., 179 days TOT, $p < 0.001$), again meaning faster decomposition under continuous wetting. This was true in both burial (continuous wet $k = 0.0374 \text{ day}^{-1}$ i.e., 26.7 days TOT and wet-dry $k = 0.00372$ i.e., 268 days TOT) and erosional ($k = 0.0377 \text{ day}^{-1}$ i.e., 26.5 days TOT and wet-dry $k = 0.00746 \text{ day}^{-1}$ i.e., 134 days TOT) transects, as well as Brady (continuous wet $k = 0.0376 \text{ day}^{-1}$ i.e., 26.6 days TOT and wet-dry $k = 0.00871 \text{ day}^{-1}$ i.e., 115 days TOT) and modern (continuous wet $k = 0.0375 \text{ day}^{-1}$ i.e., 26.7 days TOT and wet-dry $k = 0.00248 \text{ day}^{-1}$ i.e., 404 days TOT) soils.

With the two-pool models, the decay rate of the slow-cycling SOM pool in the continuously wet experiment was significantly lower ($1.11 \cdot 10^{-5} \text{ day}^{-1}$ i.e., 246 years TOT) than that of the wet-dry cycling experiment (0.00812 day^{-1} i.e., 123 days TOT, $p < 0.001$), reflecting faster turnover in the wet-dry treatments. This was true in both Brady (continuously wet $k = 6.86 \cdot 10^{-6} \text{ day}^{-1}$ i.e., 399 years TOT, wet-dry $k = 0.0083 \text{ day}^{-1}$ i.e., 120 days TOT) and modern (continuously wet $k = 1.54 \cdot 10^{-5} \text{ day}^{-1}$ i.e., 178 years TOT, wet-dry $k = 0.00793 \text{ day}^{-1}$ i.e., 126 days TOT) soils, as well as both burial (continuously wet $k = 8.68 \cdot 10^{-6} \text{ day}^{-1}$ i.e., 316 years TOT, wet-dry $k = 0.00773 \text{ day}^{-1}$ i.e., 129 days TOT) and erosional (continuously wet $k = 1.36 \cdot 10^{-5} \text{ day}^{-1}$ i.e., 202 years TOT, wet-dry $k = 0.0085 \text{ day}^{-1}$ i.e., 118 days TOT) transects, and at all degrees of burial and erosional exposure.

The decay rate of the fast-cycling SOM pool in modern soil was significantly higher in the wet-dry cycling experiment (8.11 day^{-1} i.e., 0.123 days TOT) compared to the continuously wet experiment (0.127 day^{-1} i.e., 7.89 days TOT, $p < 0.001$), indicating a much faster turnover response to rewetting. The decay rate of the fast-cycling pool in the erosional transect was also significantly higher in the wet-dry cycling experiment (5.148 day^{-1} i.e., 0.194 days TOT) compared to the continuously wet

599 experiment (0.130 day^{-1} i.e., 7.68 days TOT). Separating these effects by degree of
600 erosional exposure revealed that the significance of the difference between the fast pool
601 decay rate in modern soils was more evident at the intermediate and lowest degree
602 of erosion. The decay rate of the fast-cycling SOM pool did not differ significantly
603 between continuously wet and wet-dry cycling experiments in Brady soils or in the
604 burial transect.

605 Among the control soils with two-pool models, the continuous wet experiment had
606 significantly lower slow pool decay rate ($1 \cdot 10^{-8} \text{ day}^{-1}$ i.e., 274 000 years TOT)
607 compared to the wet-dry cycling experiment ($k = 0.005 \text{ day}^{-1}$ i.e., 200 days TOT, p
608 < 0.01), again corresponding to much faster turnover in the wet-dry treatments. This
609 was true in both the burial and erosional transects, modern and Brady Soil and at all
610 degrees of erosion and burial.

611 In contrast to the main soil dataset described above, the decay rate of the fast-
612 cycling SOM pool of control Brady Soil was significantly higher in the wet-dry cycling
613 experiment (0.0556 day^{-1} i.e., 18.0 days TOT) compared to the continuously wet
614 experiment (10.3 day^{-1} i.e., 0.0971 days TOT). This was true in both burial and
615 erosional transects. In modern control soils, however, there was no significant difference
616 between decay rates of fast-cycling SOM in continuously wet versus wet-dry cycling
617 experiments.

618 The fraction size of the slow-cycling SOM pool in the wet-dry cycling experiment
619 was significantly larger (0.999) than that of the continuously wet experiment (0.987, p
620 < 0.001) - this was true for both Brady and modern soils, across erosional and burial
621 transects and at all degrees of erosion and burial. It follows that the fraction size of
622 the fast-cycling SOM pool in wet-dry cycling experiments was significantly smaller
623 (0.001) than that of the continuously wet experiment (0.0131, $p < 0.001$) for soils of
624 all transect types, paleostatus groups and degrees of erosion and burial. There was
625 no significantly difference between fraction sizes of the slow-cycling SOM pool among
626 the controls of the wet-dry cycling and continuously wet experiment; the fast-cycling
627 pool was also similar among control soils of the two experiments.

629 3.6 Relationships between soil properties and carbon dynamics

630 The true versus predicted values MLR models for prediction of decomposition rates of
631 the fast- and slow-cycling pools as well as the fraction size of the slow pool are shown
632 in the Appendix, Fig. A2. A matrix showing the correlation between these variables is
633 given in Fig. 6. The intercept, coefficients of explanatory variables, RMSE and R^2 of
634 the best-performing MLR models, are summarized in Table 3 and the full equations
635 are in the Appendix (Multiple linear regression equations).

636 The MLR models for prediction of decay rates of SOM under continuous wetting
637 had better model fit ($R^2 > 0.80$) compared to those for predictions of SOM pool
638 fraction size ($R^2 = 0.44$). From the MLR equations, we deduce that soil properties with
639 the greatest coefficients had the most important effects on the SOM decay rate and
640 fraction size model parameters. While SAR increased the rate of decay and decreased
641 the size of the of the slow pool, an opposite trend is observed in the fast pool.

642 TOC and pH also increased the decay rate of the fast-cycling SOM pool under
643 continuous wetting, while the slow pool decay rate decreased with increasing TIC.
644

TOC and TIC increased the fraction size of the slow pool at the expense of fraction size of the fast pool. When considering effects of these factors individually, SAR, TOC, TIC and pH did not have significant correlation with SOM decomposition parameters (Fig. 6). However, exchangeable Mg and K content were significantly correlated with the decay rate of the fast (negative correlation) and slow (positive correlation) pools (Fig. 6).

The true versus predicted values MLR models for prediction of the decomposition rate of SOM (one-pool system) under wet-dry cycles are shown in the Appendix, Fig A3. A matrix showing the correlation between these variables is given in Appendix, Fig. A4.

The intercept, coefficients of explanatory variables, RMSE and R^2 of the best-performing MLR model for prediction of the decay rate, are given summarized in Table 3 and the full equation is in the Appendix (Multiple linear regression equations).

SAR decreased the decay rate of SOM under wet-dry cycles. Clay and TOC content increased the decay rate of SOM. Exchangeable Ca, Mg content decreased the decay rates of both pools. Considering these parameters individually (correlation coefficients) revealed a weak correlation with k. Therefore MLR, where k is modeled as a function of all predictors together, demonstrates that the combination of these variables explained most variance, while no single predictor explained much variance on its own.

4 Discussion

4.1 Stabilization of soil organic matter by burial

While our study characterizes decomposition dynamics using respirometry and radiocarbon-based modeling, we did not directly measure the molecular mechanisms responsible for differential SOC stability. Specifically, we did not quantify the chemical composition of mineral-associated organic matter, the nature of organo-mineral bonds, or microbial community composition. As a result, the mechanistic interpretations presented here are necessarily indirect.

The interpretations proposed in this study build on prior molecular and fractionation-based analyses conducted on the same soils and geomorphic transects (Marin-Spiotta et al. 2014; Dolui et al. 2026b). That work documented enhanced mineral association and cation-mediated stabilization in buried profiles. Rather than repeating those analyses, the present study extends this framework by quantifying how these stabilization contexts translate into differences in SOC turnover rates and pool structure under contrasting moisture regimes.

Brady Soil subjected to continuous wetting exhibited lower cumulative CO_2 evolution than modern soils across both erosional and burial transects (Fig. 2; Appendix Fig. 3). This pattern indicates reduced microbial mineralization in buried paleosols relative to surface soils under sustained moisture availability.

Multiple mechanisms may contribute to this enhanced stability, although their relative importance cannot be resolved with the current dataset. Previous work at this site reported elevated exchangeable Ca^{2+} concentrations in Brady soils and linked Ca-mediated flocculation to increased aggregate stability (Dolui et al. 2026a). Our results are consistent with this interpretation. Specifically, Ca concentration was a

691 positive predictor of slow-pool size in the MLR model. However, we did not directly
692 measure aggregation or flocculation processes. As a result, the pathway linking Ca
693 availability to reduced decomposition remains uncertain. Reduced decay could arise
694 from physical protection within aggregates, reduced microbial access to substrates, or
695 changes in solute diffusivity (Six et al. 2002). Within the scope of this study, Ca²⁺
696 therefore emerges as a statistically robust predictor of SOC pool structure, rather than
697 a resolved mechanistic driver.

698 The potential contribution of pyrogenic carbon to SOC persistence in Brady soils
699 is supported by prior molecular analyses from this site. These analyses identified con-
700 densed aromatic compounds consistent with fire-derived inputs (Marin-Spiotta et al.
701 2014). Pyrogenic carbon was not quantified in the present study, and its direct influ-
702 ence on decomposition rates cannot be evaluated here. Nonetheless, its documented
703 persistence provides important context for interpreting the slow-cycling SOC pool
704 observed in Brady soils. Our results are therefore compatible with a stabilization legacy
705 established during Brady Soil formation, rather than evidence of an active pyrogenic
706 control on contemporary decomposition.

707 Modern soils exhibited a slightly larger relative size of the fast-cycling SOM pool
708 than Brady soils, which likely reflects recent organic inputs. Direct comparison of
709 decay parameters further highlights differences in SOM persistence between soil types
710 (Fig. 4). The slow-cycling pool in Brady soils from the most erosional transect had
711 significantly lower decay rates under continuous wetting than the corresponding pool in
712 modern soils. This provides clear evidence of greater SOM persistence in the paleosol.

713 Across all treatments, the slow pool decayed approximately 2000 times more slowly
714 than the fast pool (Appendix, Fig. A2). The slow-cycling pool of the Brady Soil exhib-
715 ited a turnover time (TOTs) of approximately 399 years, whereas the slow-cycling pool
716 of modern soil exhibited a TOT of approximately 178 years. The MLR models further
717 showed a negative relationship between slow-pool decay rate (k_{slow}) and both total
718 inorganic carbon (TIC) and exchangeable Mg²⁺ (Equation A1). Although CaCO₃
719 cementation was not pronounced, positive correlations between TOC, TIC, and Ca
720 in Brady soils from erosional transects (Dolui et al. 2026a) suggest that carbonate-
721 associated phases may contribute to stabilization where shallow wetting promotes
722 near-surface carbonate precipitation.

723 The association between finer texture and reduced SOC decomposition observed in
724 this study aligns with established theory linking clay-rich soils to enhanced mineral-
725 associated organic matter formation (Six et al. 2002). Clay content was a significant
726 predictor of slow-pool dynamics in the MLR models, indicating that particle size exerts
727 a first-order control on SOC accessibility. However, because mineral surface chemistry
728 and sorption energetics were not resolved, texture is interpreted here as a proxy for
729 stabilization potential rather than as a direct mechanistic control, given the complexity
730 of detangling texture and mineralogical controls (Rasmussen et al. 2018).

731 The slow-cycling SOM pool dominated total soil C, accounting for more than
732 96% of SOC (Fig. 4b). The size of this pool increased with increasing TOC and TIC
733 (Equation A1) and was accompanied by a corresponding decline in the fast-cycling
734 pool. The fast pool consistently represented a larger fraction of total SOC in modern
735 soils than in Brady soils, and in erosional transects than in burial transects. Together,
736

these patterns indicate stronger stabilization in buried paleosols and underscore the central role of the slow-cycling pool in long-term SOC persistence.

Apparent relationships between sodium adsorption ratio (SAR), exchangeable cations, decay rates, and pool sizes in the MLR models (Equations A1, A2, A3, and A4; Fig. 6) should be interpreted cautiously. These correlations may reflect shared depth-dependent trends rather than direct mechanistic links. Both TOC and microbial biomass typically decline with depth (Fierer and Schimel 2003; Xiang et al. 2008), which contributes to reduced respiration in deeper Brady soils. At the same time, Na tends to accumulate at depth through leaching (Dolui et al. 2026a), with accumulation depth depending on precipitation and soil water status.

4.2 Destabilization of SOM by erosion and moisture variability

Greater cumulative C loss from shallower soils, combined with a smaller fast-cycling SOM pool and a significantly higher slow-pool decay rate in erosional Brady soils compared to burial Brady soils (Fig. 4a), highlights the destabilizing effect of surface exposure. This pattern indicates that erosion weakens burial-associated protection.

CO₂ pulses during the initial phase of wet–dry cycling were larger in erosional transects than in burial transects (Fig. A1). These pulses suggest enhanced mineralization in Brady soils closer to the surface. One likely explanation is priming by root exudates and fresh organic inputs, amplified by bioturbation (Pausch et al. 2016; McMurtry et al. 2024). This interpretation is supported by higher fraction modern values in erosional Brady soils relative to burial Brady soils, as well as by convergence of slow-pool fraction modern values toward those of modern soils (Dolui et al. 2026b).

Enhanced decomposition in shallower Brady soils likely reflects both legacy exposure and contemporary environmental conditions. Shallower positions experience more frequent wetting and greater oxygen diffusion, which can prime microbial communities for rapid response following rewetting. Separating long-term exposure effects from ongoing environmental controls would require experimental manipulation of burial depth, which represents an important avenue for future research.

In the wet–dry experiment, erosion effects were further expressed in decay dynamics. Slow pools decayed faster in erosional transects than in burial transects, whereas fast pools decomposed more rapidly in modern soils than in Brady soils. The fraction of the slow pool was smaller under continuous wetting than under wet–dry cycling, indicating greater allocation to slow-cycling carbon under variable moisture. However, the slow pool also exhibited substantially higher decay rates under wet–dry cycling. This suggests that apparent stabilization under variable moisture is transient and may be offset over time by depletion of passive C reserves.

The accelerated decay of slow-pool SOC under drying–rewetting cycles demonstrates that burial-associated protection is not absolute, even for millennially persistent carbon. Potential mechanisms include aggregate disruption, increased solute transport, or shifts in microbial accessibility. While the present study cannot resolve these pathways, it clearly documents the outcome: enhanced decomposition of previously slow-cycling SOC under moisture variability.

783 Moisture variability also amplified turnover of the fast-cycling pool. Decay rates
784 of the fast pool increased under wet–dry cycling, particularly in modern soils and ero-
785 sional transects. This pattern supports the interpretation that fresh organic inputs and
786 surface exposure accelerate labile C turnover under fluctuating moisture. The MLR
787 model reinforces this interpretation by revealing a positive relationship between TOC
788 and fast-pool decay rate (Equation A4). In contrast, the absence of strong moisture
789 effects in Brady soils suggests that burial dampens moisture-driven variability in labile
790 C decomposition.

791 McDowell et al. (2022) simulated soil hydrology for the Brady Soil, overlying loess,
792 and modern soil using measured hydraulic properties and regional weather data from
793 2009–2019. Modeled water contents remained low and relatively constant below 1.5 m
794 depth from the surface, including within the Brady Soil, with only rare deep wetting
795 events following major rainfall. Paleoclimate reconstructions indicate that the depth
796 of frequent wetting would have been even shallower during drier-than-modern periods
797 over the past 10,000 years (Miao et al. 2007). Together, these results suggest that
798 prolonged dry conditions played a major role in OC sequestration where the Brady
799 Soil is deeply buried, whereas erosion and increased moisture variability could promote
800 renewed C loss.

801 Geomorphic position integrates multiple stabilization controls by regulating burial
802 depth, moisture exposure, oxygen availability, and the persistence of mineral–organic
803 associations. In this sense, geomorphic context operates as a higher-order constraint
804 that modulates how chemical and physical stabilization mechanisms are expressed
805 through time. This aligns with conceptual frameworks suggesting that spatial patterns
806 of soil organic carbon (SOC) are fundamentally shaped by the interplay between bio-
807 logical cycling and geomorphic processes like erosion and deposition (Yoo et al. 2006).
808 Furthermore, topography acts as a primary control on SOC distribution by mediating
809 local microclimate and the lateral transport of soil material across mantled landscapes
810 (Patton et al. 2019). These findings challenge the common assumption in soil carbon
811 modeling that geomorphic context can be neglected when parameterizing decompo-
812 sition rates. Recent evidence underscores that geomorphic settings not only dictate
813 the abundance of SOC but also the persistence of specific carbon pools, particularly
814 in erosional landscapes where geomorphic history defines the vulnerability of buried
815 carbon (Hunter et al. 2024). Our results show that erosional exposure accelerates slow-
816 pool decay under continuous wetting, and that wet–dry cycling destabilizes slow-pool
817 carbon regardless of landscape position. For Earth system models that treat subsoil
818 carbon as a passive reservoir, these dynamics represent a substantial and underappre-
819 ciated vulnerability. Accurately predicting SOC responses to changing precipitation
820 regimes therefore requires explicit consideration of burial depth and exposure history,
821 which are rarely incorporated into current modeling frameworks.

822

823 5 Conclusion

824

825 When interpreted alongside prior molecular- and fractionation-based analyses from
826 this site (Marin-Spiotta et al. 2014; Dolui et al. 2026a,b), our results suggest that long-
827 term SOC persistence in Brady soils arises from the convergence of mineral association,
828

cation-mediated stabilization, and limited environmental exposure. The present study extends this framework by demonstrating that these stabilization contexts remain vulnerable to hydrologic perturbation and geomorphic re-exposure. Although this study does not resolve molecular-scale mechanisms directly, it demonstrates that decomposition parameters derived from incubation and radiocarbon modeling are highly sensitive to landscape history – an effect that must be accounted for even when detailed chemical data are unavailable.

Our study demonstrates that SOC decomposition is strongly shaped by soil moisture regime and landscape position, with modern and Brady soils responding differently to continuous wetting versus drying–rewetting cycles. Water availability exerted disproportionate effects in erosional settings where surface exposure enhanced substrate diffusivity, highlighting the destabilizing role of re-exposure and moisture fluctuations.

Drying–rewetting cycles led to greater C losses from Brady soils than continuous wetting, despite modeling results indicating dominance of the slow pool and depletion of labile C. This treatment also accelerated fast pool decay in modern soils and erosional transects, while burial dampened such variability in Brady soils. Fraction sizes shifted accordingly: wet–dry cycles increased the proportion of the slow pool and reduced the fast pool fraction, suggesting redistribution of SOC toward more stabilized forms under fluctuating moisture.

Depth further constrained SOM persistence, with slow pool decay constants declining with increasing degree of burial in Brady soils from burial transects. Faster turnover in shallow layers reflects greater microbial accessibility and responsiveness to surface-driven processes, underscoring the importance of geomorphic context - transect type, degree of burial, and soil structure - over intrinsic SOM chemistry.

Comparisons across models showed that continuous wetting accelerated overall decay, particularly in burial transects, while wet–dry cycles disproportionately destabilized the slow pool that dominates SOC. This dual effect - rapid labile C turnover under moisture fluctuations coupled with erosion of long-lived SOM persistence - points to heightened vulnerability of buried carbon under future precipitation variability.

Overall, the fate of ancient soil carbon under climate change will depend on both its burial history and prevailing moisture regime. Integrating these contrasting controls on fast- and slow-cycling pools into Earth system models is essential for improving predictions of soil carbon vulnerability and climate feedback.

Funding. This work was supported by the National Science Foundation (EAR awards 1623814, 1623810, and 1623812), the University of California, Merced, and the Ted and Jan Falasco Endowment.

Competing interests. The authors have no relevant financial or non-financial interests to disclose.

Data availability. Full dataset for soil incubation and statistical analyses are available at DOI: [doi: 10.17632/fjw646gpyf.1](https://doi.org/10.17632/fjw646gpyf.1).

875 **Author contributions.** All authors contributed to the study conception and
876 design. Material preparation, data collection, and analysis were performed by Man-
877 isha Dolui, Teneille Nel, Abbygail R. McMurtry, Stephanie Chacon, Laura M. Phillips,
878 Teamrat Ghezzehei, Joseph A. Mason, Erika Marin-Spiotta, Marie-Anne de Graaff
879 and Asmeret Asefaw Berhe. The first draft of the manuscript was written by Manisha
880 Dolui and Teneille Nel. All authors commented on previous versions of the manuscript
881 and approved the final manuscript.

882 **Acknowledgments.** We acknowledge financial support for this work from the
883 National Science Foundation (EAR awards 1623814, 1623810, and 1623812) and the
884 Ted and Jan Falasco Endowment, fellowships and grants awarded by the Graduate
885 Division at the University of California, Merced (UCM), and the UCM Environmen-
886 tal Systems Graduate Group. We are grateful to Dr. Sora Kim and Dr. Robin Trayler
887 for their support at the UCM Stable Isotope Lab. We also thank R. and D. Whiting
888 for providing access to the Wauneta, Nebraska, field sites. ChatGPT was used for lan-
889 guage editing and sentence refinement and the authors take full responsibility for the
890 output.
891
892
893
894
895
896
897
898
899
900
901
902
903
904
905
906
907
908
909
910
911
912
913
914
915
916
917
918
919
920

Tables and figures.

921
922
923
924
925
926
927
928
929
930
931
932
933
934
935
936
937
938
939
940
941
942
943
944
945
946
947
948
949
950
951
952
953
954
955
956
957
958
959
960
961
962
963
964
965
966

967
 968
 969
 970
 971
 972
 973
 974
 975
 976
 977
 978
 979
 980
 981
 982
 983
 984
 985
 986
 987
 988
 989
 990
 991
 992
 993
 994
 995
 996
 997
 998
 999
 1000
 1001
 1002
 1003
 1004
 1005
 1006
 1007
 1008
 1009
 1010
 1011
 1012

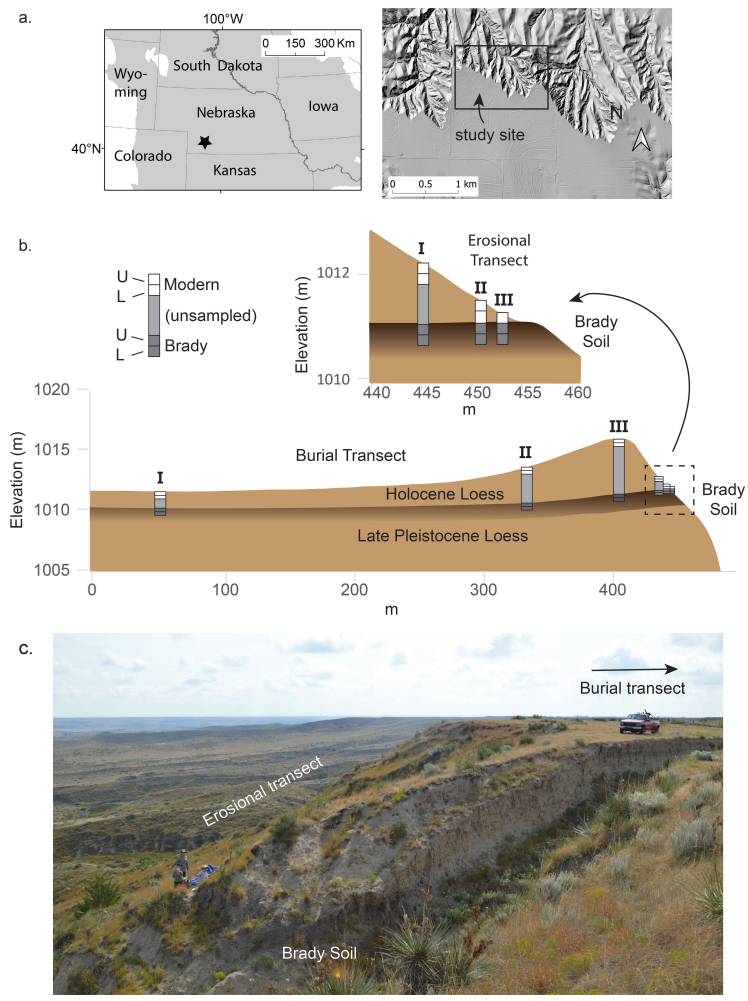


Fig. 1 Study site location, stratigraphy, and sampling scheme. a. Location of the study site within the Great Plains ecoregion (grayshade) and shaded relief map illustrating topographic setting of study site. b. Vertical cross-sections illustrating the sampling scheme relative to modern land surface topography, the Brady Soil, and loess above and below it at study site. Weakly developed horizons of modern soil and paleosols within the Holocene loess (Miao et al., 2007) not shown. Details based on one pair of burial and erosional transects but representative of all three. c. Photo illustrating topography and native grassland vegetation at one pair of transects. Truck is near deepest profile (III) on burial transect; other burial transect points are not visible. Brady Soil is exposed in an old roadcut in foreground; erosional transect is located on intact slope beyond roadcut. Figure adapted from [Dolui et al. \(2026b\)](#)

1013
 1014
 1015
 1016
 1017
 1018
 1019
 1020
 1021
 1022
 1023
 1024
 1025
 1026
 1027
 1028
 1029
 1030
 1031
 1032
 1033
 1034
 1035
 1036
 1037
 1038
 1039
 1040
 1041
 1042
 1043
 1044
 1045
 1046
 1047
 1048
 1049
 1050
 1051
 1052
 1053
 1054
 1055
 1056
 1057
 1058

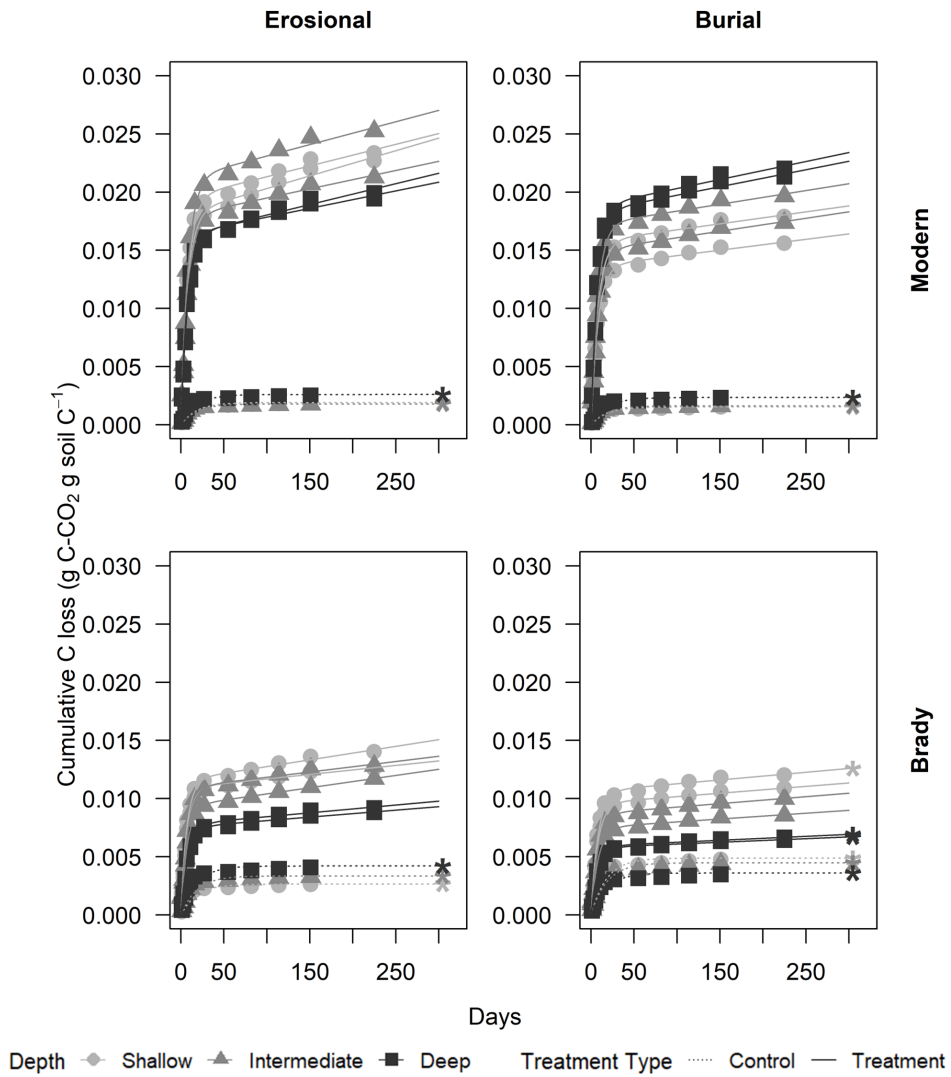


Fig. 2 Cumulative respiratory CO₂ from modern and Brady Soil sampled from three depths representing varying degrees of burial/erosional exposure (two technical replicates each). In burial transects, Shallow → Intermediate → Deep corresponds to burial degrees I → II → III. In erosional transects, this relationship is reversed, with Shallow → Intermediate → Deep corresponding to exposure degrees III → II → I. Soils were maintained at a constant moisture content of 60% water holding capacity (WHC). Lines depict a two-pool first-order decay model, fitted using a non-linear least-squares function. The dotted line represents the control (5% WHC).

1059
 1060
 1061
 1062
 1063
 1064
 1065
 1066
 1067
 1068
 1069
 1070
 1071
 1072
 1073
 1074
 1075
 1076
 1077
 1078
 1079
 1080
 1081
 1082
 1083
 1084
 1085
 1086
 1087
 1088
 1089
 1090
 1091
 1092
 1093
 1094
 1095
 1096
 1097
 1098
 1099
 1100
 1101
 1102
 1103
 1104

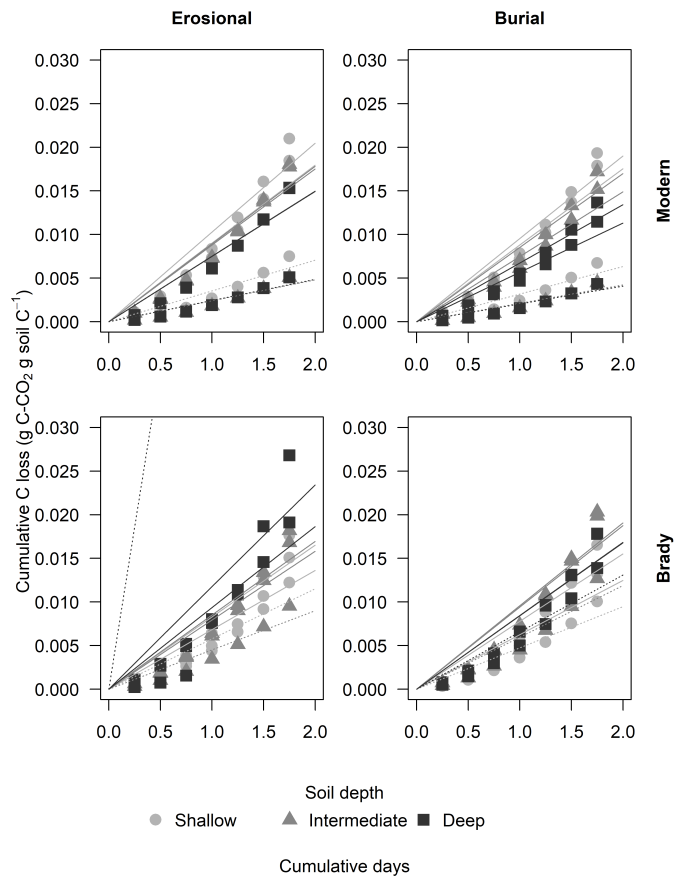


Fig. 3 Cumulative respiratory CO₂ flux from modern and Brady Soil sampled from three depths representing varying degrees of burial/erosional exposure (two technical replicates each). In burial transects, Shallow → Intermediate → Deep corresponds to burial degrees I → II → III. In erosional transects, this relationship is reversed, with Shallow → Intermediate → Deep corresponding to exposure degrees III → II → I. Soils were wetted to a moisture content of 60% water holding capacity (WHC) and allowed to dry to 5% WHC. Lines depict a one-pool first-order decay model, fitted using a non-linear least-squares function. The dotted line represents the control (constant 5% WHC); one control Brady soil sample of the erosional transect had an outlier point not shown due to scale. Asterisks (*) indicate control samples maintained at 5% WHC

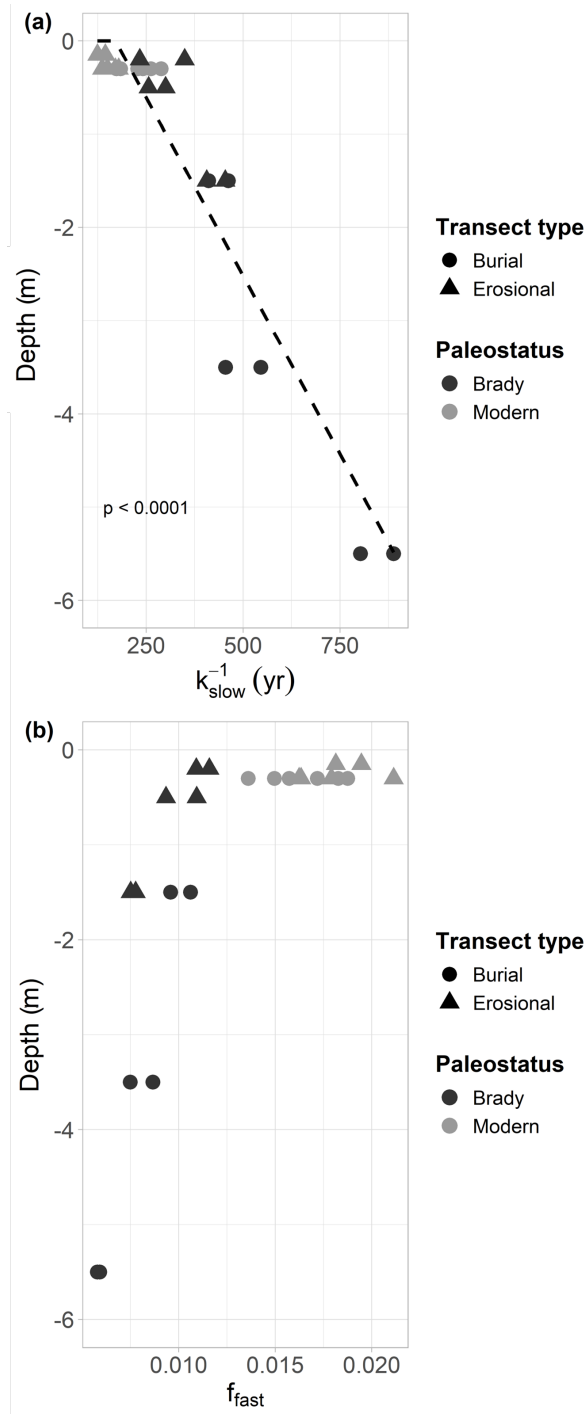


Fig. 4 Decay constant of the slow cycling pool of modern and Brady soils at different depths (from the soil surface), incubated under continuously wet conditions. Samples collected from burial and erosional transect types. Dotted line indicates exponential decay. Figure b indicates the size of the fast-cycling pool at different depths (from the soil surface) of the modern and Brady soils in burial and erosional transect types.

1105
 1106
 1107
 1108
 1109
 1110
 1111
 1112
 1113
 1114
 1115
 1116
 1117
 1118
 1119
 1120
 1121
 1122
 1123
 1124
 1125
 1126
 1127
 1128
 1129
 1130
 1131
 1132
 1133
 1134
 1135
 1136
 1137
 1138
 1139
 1140
 1141
 1142
 1143
 1144
 1145
 1146
 1147
 1148
 1149
 1150

1151
1152
1153
1154
1155
1156
1157
1158
1159
1160
1161
1162
1163
1164
1165
1166
1167
1168
1169
1170
1171
1172
1173
1174
1175
1176
1177
1178
1179
1180
1181
1182
1183
1184
1185
1186
1187
1188
1189
1190
1191
1192
1193
1194
1195
1196

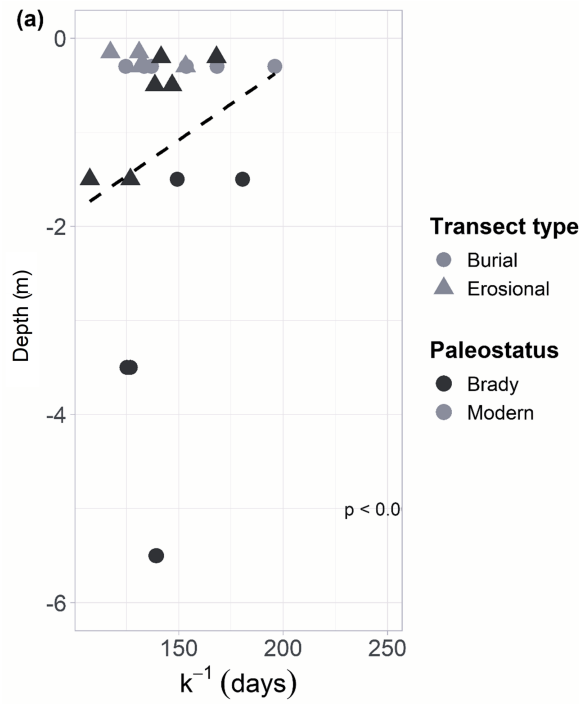


Fig. 5 Decay constant of the slow cycling pool of modern and Brady soils at different depths (from the soil surface), incubated under wet-dry cycling conditions. Samples collected from burial and erosional transect types. Dotted line indicates exponential decay.

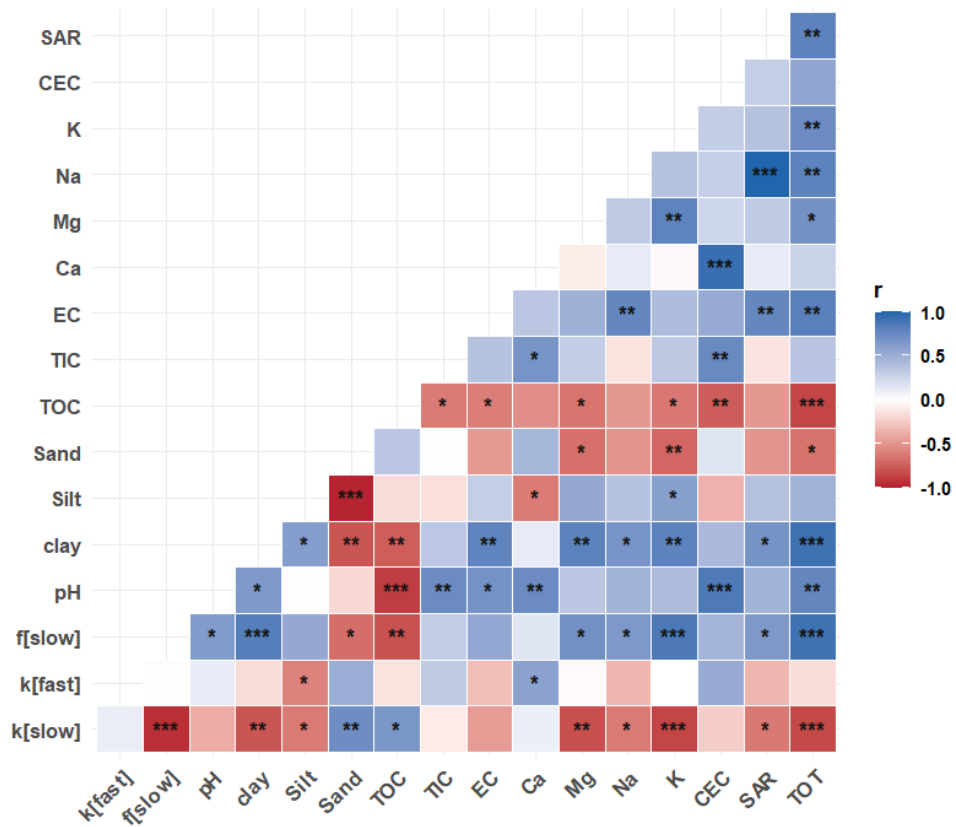


Fig. 6 Correlation between soil physicochemical properties and modeled soil organic matter decomposition parameters (decay constant, k , and fraction of C in slow pool, f) for fast- and slow-cycling pools in modern and Brady soils incubated under continuously wet conditions. Decomposition parameters were obtained by multiple linear regression across burial and erosional transects. The statistical significance of each correlation is denoted by asterisks (*** for $p < 0.001$, ** for $p < 0.01$, * for $p < 0.05$).

1243
1244
1245
1246
1247
1248
1249
1250
1251
1252
1253
1254
1255
1256
1257
1258
1259
1260
1261
1262
1263
1264
1265
1266
1267
1268
1269
1270
1271
1272
1273
1274
1275
1276
1277
1278
1279
1280
1281
1282
1283
1284
1285
1286
1287
1288

Table 1 General physicochemical (mean \pm standard deviation) of soils used in the incubation experiment, grouped by transect type and paleostatus

Transect type Paleostatus	Burial		Erosional	
	Brady	Modern	Brady	Modern
pH	7.77 \pm 0.04	6.89 \pm 0.32	7.68 \pm 0.12	7.41 \pm 0.10
Clay (%)	9.48 \pm 0.75	6.13 \pm 0.64	7.62 \pm 0.44	6.29 \pm 0.48
Silt (%)	59.31 \pm 0.44	56.24 \pm 5.76	55.73 \pm 4.88	53.67 \pm 1.51
Sand (%)	31.24 \pm 0.94	37.62 \pm 6.39	36.64 \pm 5.22	40.08 \pm 1.92
TOC content	0.45 \pm 0.06	1.03 \pm 0.20	0.56 \pm 0.10	0.93 \pm 0.17
TIC content	0.24 \pm 0.11	0.09 \pm 0.03	0.28 \pm 0.04	0.25 \pm 0.03
EC (dS m ⁻¹)	5.41 \pm 0.32	2.26 \pm 0.43	3.05 \pm 0.47	3.57 \pm 0.35
CEC (cmolc kg ⁻¹)	22.86 \pm 0.54	15.17 \pm 3.54	23.31 \pm 3.52	20.59 \pm 1.83
Turnover time (y)	15654 \pm 2440	576.4 \pm 126	8327 \pm 2732	1451 \pm 673
CN ratio	10.00 \pm 0.45	9.24 \pm 0.21	10.96 \pm 0.20	9.76 \pm 0.25

1289
1290
1291
1292
1293
1294
1295
1296
1297
1298
1299
1300
1301
1302
1303
1304
1305
1306
1307
1308
1309
1310
1311
1312
1313
1314
1315
1316
1317
1318
1319
1320
1321
1322
1323
1324
1325
1326
1327
1328
1329
1330
1331
1332
1333
1334

Table 2 Soil organic matter (SOM) decomposition parameters (decay rate k of one-pool model, decay rates of fast- (k_{fast}) and slow-cycling (k_{slow}) SOM pools, and fraction sizes of fast (f_{fast}) and slow (f_{slow}) pools, grouped by experiment, transect type, and paleostatus.

Experiment	CW				WD			
	Burial		Erosional		Burial		Erosional	
Transect type	Brady	Modern	Brady	Modern	Brady	Modern	Brady	Modern
Paleostatus	Brady	Modern	Brady	Modern	Brady	Modern	Brady	Modern
k (one pool)	0.0107	0.0099	0.0069	0.0072	0.0071	0.0067	0.0074	0.0074
k_{slow}	<0.0001	<0.0001	<0.0001	<0.0001	0.0080	0.0074	0.0086	0.0084
k_{fast}	0.1250	0.1264	0.1333	0.1270	6.6931	6.3419	0.4222	9.8728
f_{slow}	0.9920	0.9836	0.9903	0.9818	0.9990	0.9990	0.9990	0.9990
f_{fast}	0.0080	0.0164	0.0097	0.0182	0.0010	0.0010	0.0010	0.0010

1335
1336
1337
1338
1339
1340
1341
1342
1343
1344
1345
1346
1347
1348
1349
1350
1351
1352
1353
1354
1355
1356
1357
1358
1359
1360
1361
1362
1363
1364
1365
1366
1367
1368
1369
1370
1371
1372
1373
1374
1375
1376
1377
1378
1379
1380

Table 3 Summary of multiple linear regression models showing key positive (+) and negative (-) predictors of model parameters (proportions of fast and slow cycling fractions of TOC, i.e., f_f and f_s and the corresponding decay rate constants k_f and k_s), model performance (R^2), and root mean square error (RMSE).

Model parameter	Key (+) predictors	Key (-) predictors	R^2	RMSE
k_{slow}	clay, Ca, EC	SAR, Mg, K, pH, TOC, TIC	0.98	7.01×10^{-7}
k_{fast}	SAR, clay, Ca, Mg, TIC	K, EC, pH	0.95	1.41×10^{-3}
f_{slow}	SAR, Mg, K, pH, TIC	clay, Ca, EC, TOC	0.97	8.38×10^{-4}
f_{fast}	clay, Ca, EC, TOC	SAR, Mg, K, pH, TIC	0.97	8.38×10^{-4}
$k_{one-pool}$	clay, K, pH, TOC	SAR, Ca, Mg	0.94	2.15×10^{-4}

Appendix A

1381
1382
1383
1384
1385
1386
1387
1388
1389
1390
1391
1392
1393
1394
1395
1396
1397
1398
1399
1400
1401
1402
1403
1404
1405
1406
1407
1408
1409
1410
1411
1412
1413
1414
1415
1416
1417
1418
1419
1420
1421
1422
1423
1424
1425
1426

1427
 1428
 1429
 1430
 1431
 1432
 1433
 1434
 1435
 1436
 1437
 1438
 1439
 1440
 1441
 1442
 1443
 1444
 1445
 1446
 1447
 1448
 1449
 1450
 1451
 1452
 1453
 1454
 1455
 1456
 1457
 1458
 1459
 1460
 1461
 1462
 1463
 1464
 1465
 1466
 1467
 1468
 1469
 1470
 1471
 1472

Table A1 Absolute sampling depth intervals i.e., depth from soil surface (standard deviation in brackets for $n = 3$) of modern (surface) and Brady (burial) soils along two types of transects, where degrees of burial or exposure increase from degrees I to III. Table adapted from [Dohui et al. \(2026b\)](#)

Depth (cm)	Transect Type					
	Erosional			Burial		
	III	II	I	Degree I	II	III
Modern	0-19 (2.5)	0-19 (3.2)	0-18 (3.5)	0-30 (0.6)	0-29 (0.6)	0-29 (0.0)
Paleostatus	NA	19-38 (3.6)	18-36 (3.5)	30-60 (0.6)	29-59 (2.3)	29-59 (2.3)
	20-50 (1.2)	50-80 (0.0)	150-180 (0.0)	100-130 (4.0)	300-330 (9.3)	550-580 (6.7)
	50-80 (0.4)	80-120 (0.0)	180-210 (2.9)	130-160 (4.5)	330-360 (2.6)	580-610 (5.6)
Brady						

1473
 1474
 1475
 1476
 1477
 1478
 1479
 1480
 1481
 1482
 1483
 1484
 1485
 1486
 1487
 1488
 1489
 1490
 1491
 1492
 1493
 1494
 1495
 1496
 1497
 1498
 1499
 1500
 1501
 1502
 1503
 1504
 1505
 1506
 1507
 1508
 1509
 1510
 1511
 1512
 1513
 1514
 1515
 1516
 1517
 1518

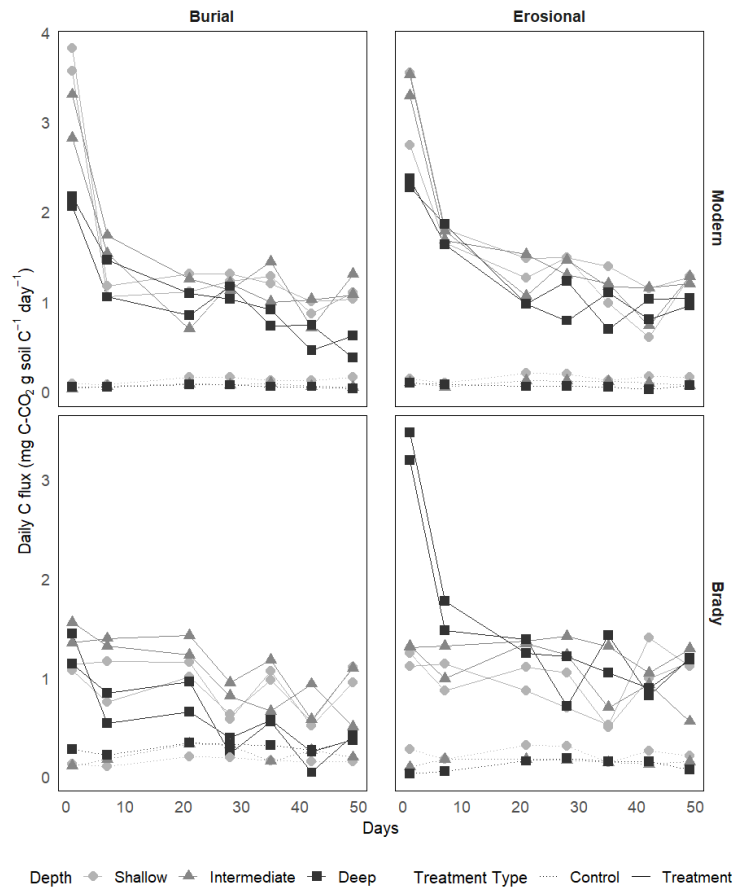


Fig. A1 Daily respiratory CO₂ flux from modern and Brady Soil sampled from three depths representing varying degrees of burial/erosional exposure (two technical replicates each). In burial transects, Shallow → Intermediate → Deep corresponds to burial degrees I → II → III. In erosional transects, this relationship is reversed, with Shallow → Intermediate → Deep corresponding to exposure degrees III → II → I. Soils were wetted to a moisture content of 60% water holding capacity (WHC) and allowed to dry to 5% WHC. The dotted line represents the control (constant 5% WHC).

1519
 1520
 1521
 1522
 1523
 1524
 1525
 1526
 1527
 1528
 1529
 1530
 1531
 1532
 1533
 1534
 1535
 1536
 1537
 1538
 1539
 1540
 1541
 1542
 1543
 1544
 1545
 1546
 1547
 1548
 1549
 1550
 1551
 1552
 1553
 1554
 1555
 1556
 1557
 1558
 1559
 1560
 1561
 1562
 1563
 1564

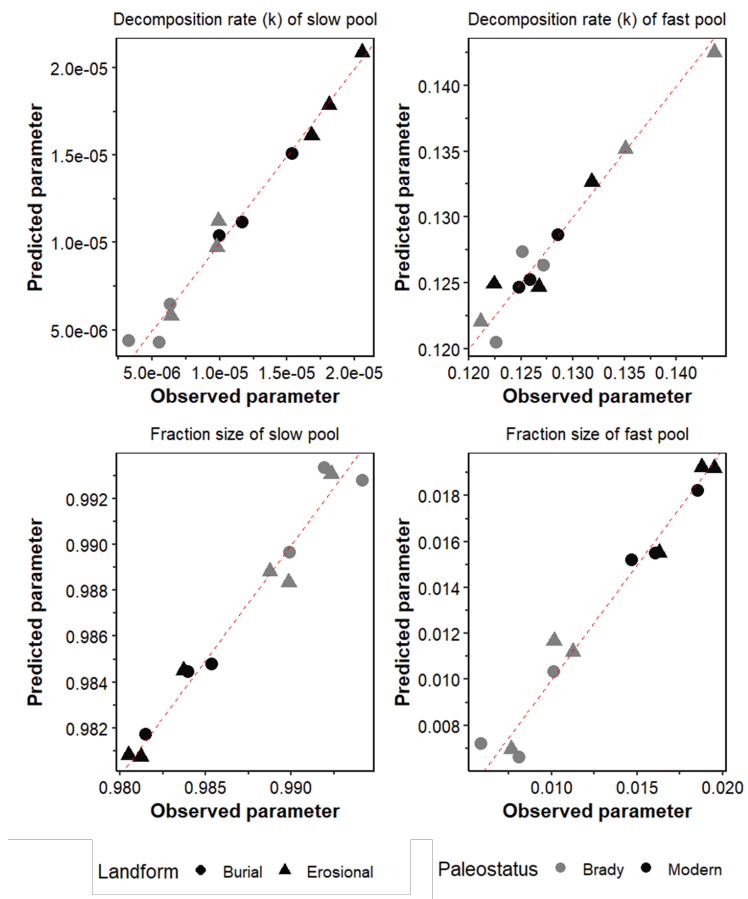


Fig. A2 True versus predicted soil organic matter decomposition parameters (decay constant, k , and fraction of C in slow pool, f) for fast- and slow-cycling pools in modern and Brady soils incubated under continuously wet conditions. These parameters were obtained by multiple linear regression across burial and erosional transects. Red dotted line represents $y = x$.

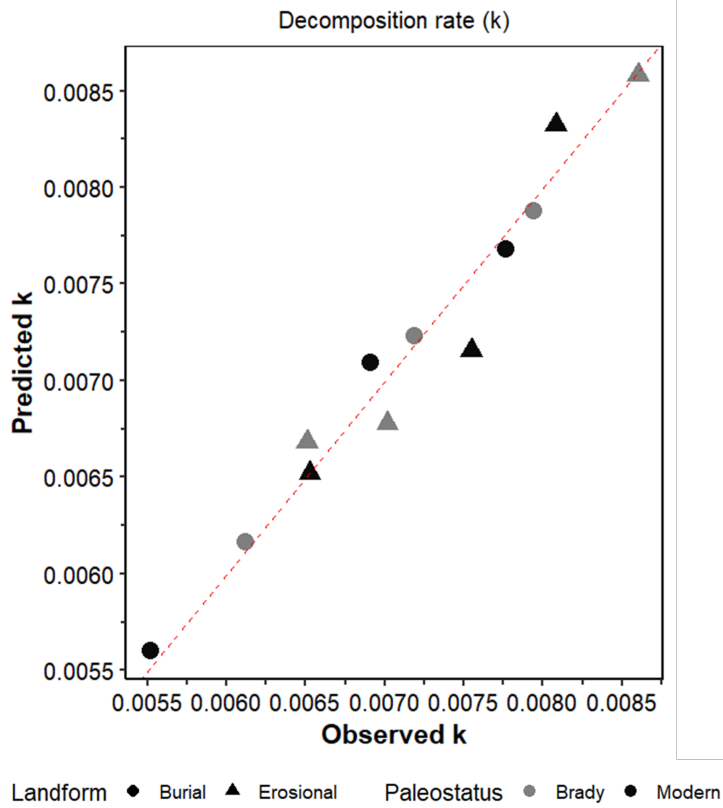


Fig. A3 True versus predicted soil organic matter decay constant, k in modern and Brady soils incubated under wet-dry cycling conditions. These parameters were obtained by multiple linear regression across burial and erosional transects. Red dotted line represents $y = x$.

1565
 1566
 1567
 1568
 1569
 1570
 1571
 1572
 1573
 1574
 1575
 1576
 1577
 1578
 1579
 1580
 1581
 1582
 1583
 1584
 1585
 1586
 1587
 1588
 1589
 1590
 1591
 1592
 1593
 1594
 1595
 1596
 1597
 1598
 1599
 1600
 1601
 1602
 1603
 1604
 1605
 1606
 1607
 1608
 1609
 1610

1611
 1612
 1613
 1614
 1615
 1616
 1617
 1618
 1619
 1620
 1621
 1622
 1623
 1624
 1625
 1626
 1627
 1628
 1629
 1630
 1631
 1632
 1633
 1634
 1635
 1636
 1637
 1638
 1639
 1640
 1641
 1642
 1643
 1644
 1645
 1646
 1647
 1648
 1649
 1650
 1651
 1652
 1653
 1654
 1655
 1656

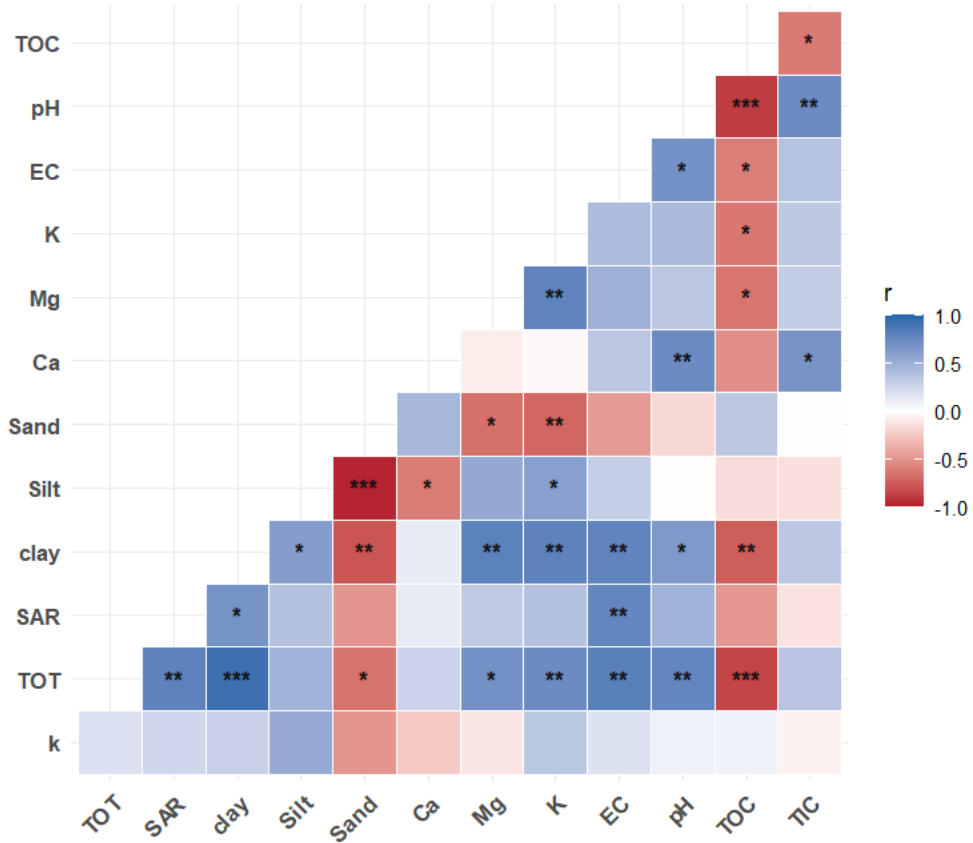


Fig. A4 Correlation between soil physicochemical properties and modeled soil organic matter decomposition parameters (decay constant, k, and fraction of C in slow pool, f) for fast- and slow-cycling pools in modern and Brady soils incubated under wet-dry cycles. Decomposition parameters were obtained by multiple linear regression across burial and erosional transects. The statistical significance of each correlation is denoted by asterisks (*** for $p < 0.001$, ** for $p < 0.01$, * for $p < 0.05$).

A.1 Multiple linear regression equations

$$\begin{aligned} k_{slow} = & 0.0000532 - 0.0000979 \cdot SAR + 0.00000225 \cdot clay + 0.000000395 \cdot Ca \\ & - 0.00000622 \cdot Mg - 0.00000271 \cdot K + 0.00000347 \cdot EC - 0.00000618 \cdot pH \\ & - 0.00000687 \cdot TOC - 0.0000275 \cdot TIC \end{aligned} \quad (A1)$$

$$RMSE : 0.000000701, \quad R^2 : 0.98$$

$$\begin{aligned} k_{fast} = & 0.215 + 0.0189 \cdot SAR + 0.00344 \cdot clay + 0.0026 \cdot Ca + 0.00204 \cdot Mg \\ & - 0.000302 \cdot K - 0.00513 \cdot EC - 0.0196 \cdot pH + 0.0146 \cdot TIC \end{aligned} \quad (A2)$$

$$RMSE : 0.00141, \quad R^2 : 0.95$$

$$\begin{aligned} f_{slow} = & 0.976 + 0.0732 \cdot SAR - 0.000362 \cdot clay - 0.000241 \cdot Ca + 0.00138 \cdot Mg \\ & + 0.00283 \cdot K - 0.00288 \cdot EC + 0.00174 \cdot pH - 0.000707 \cdot TOC \\ & + 0.0298 \cdot TIC \end{aligned} \quad (A3)$$

$$RMSE : 0.000838, \quad R^2 : 0.97$$

$$\begin{aligned} f_{fast} = & 0.0243 - 0.0732 \cdot SAR + 0.000362 \cdot clay + 0.000241 \cdot Ca - 0.00138 \cdot Mg \\ & - 0.00283 \cdot K + 0.00288 \cdot EC - 0.00174 \cdot pH + 0.000707 \cdot TOC \\ & - 0.0298 \cdot TIC \end{aligned}$$

$$RMSE : 0.000838, \quad R^2 : 0.97$$

(A4)

$$\begin{aligned} k(one - pool) = & -0.00641 - 0.00308 \cdot SAR + 0.000599 \cdot clay - 0.000141 \cdot Ca \\ & - 0.0015 \cdot Mg + 0.00118 \cdot K + 0.00159 \cdot pH \\ & + 0.002 \cdot TOC \end{aligned} \quad (A5)$$

$$RMSE : 0.000215, \quad R^2 : 0.94$$

References

Batool M, Cihacek LJ, Alghamdi RS (2024) Soil Inorganic Carbon Formation and the Sequestration of Secondary Carbonates in Global Carbon Pools: A Review. *Soil Systems* 8(1):15. <https://doi.org/10.3390/soilsystems8010015>

Beare M, Gregorich E, St-Georges P (2009) Compaction effects on CO₂ and N₂O production during drying and rewetting of soil. *Soil Biology and Biochemistry* 41(3):611–621. <https://doi.org/10.1016/j.soilbio.2008.12.024>

1703 Berhe AA, Harte J, Harden JW, et al (2007) The Significance of the Erosion-
1704 induced Terrestrial Carbon Sink. *BioScience* 57(4):337–346. [https://doi.org/10.](https://doi.org/10.1641/B570408)
1705 [1641/B570408](https://doi.org/10.1641/B570408)
1706
1707 Berhe AA, Harden JW, Torn MS, et al (2008) Linking soil organic matter dynamics
1708 and erosion-induced terrestrial carbon sequestration at different landform positions.
1709 *Journal of Geophysical Research: Biogeosciences* 113(G4). [https://doi.org/10.1029/](https://doi.org/10.1029/2008JG000751)
1710 [2008JG000751](https://doi.org/10.1029/2008JG000751)
1711
1712 Berhe AA, Suttle KB, Burton SD, et al (2012) Contingency in the direction and
1713 mechanics of soil organic matter responses to increased rainfall. *Plant and Soil*
1714 358(1-2):371–383. <https://doi.org/10.1007/s11104-012-1156-0>
1715
1716 Berhe AA, Barnes RT, Six J, et al (2018) Role of Soil Erosion in Biogeochem-
1717 ical Cycling of Essential Elements: Carbon, Nitrogen, and Phosphorus. *Annual*
1718 *Review of Earth and Planetary Sciences* 46(1):521–548. [https://doi.org/10.1146/](https://doi.org/10.1146/annurev-earth-082517-010018)
1719 [annurev-earth-082517-010018](https://doi.org/10.1146/annurev-earth-082517-010018)
1720
1721 Bird JA, Torn MS (2006) Fine Roots vs. Needles: A Comparison of ¹³C and ¹⁵N
1722 Dynamics in a Ponderosa Pine Forest Soil. *Biogeochemistry* 79(3):361–382. <https://doi.org/10.1007/s10533-005-5632-y>
1723
1724 Chaopricha NT (2013) The Importance, Origin, Composition, and Stability of Deeply
1725 Buried Soil Organic Matter. PhD thesis, University of Wisconsin-Madison, Madison
1726
1727 Chaopricha NT, Marín-Spiotta E (2014) Soil burial contributes to deep soil organic
1728 carbon storage. *Soil Biology and Biochemistry* 69:251–264. [https://doi.org/10.1016/](https://doi.org/10.1016/j.soilbio.2013.11.011)
1729 [j.soilbio.2013.11.011](https://doi.org/10.1016/j.soilbio.2013.11.011)
1730
1731 Chowdhury N, Marschner P, Burns RG (2011) Soil microbial activity and community
1732 composition: Impact of changes in matric and osmotic potential. *Soil Biology and*
1733 *Biochemistry* 43(6):1229–1236. <https://doi.org/10.1016/j.soilbio.2011.02.012>
1734
1735 Cotrufo MF, Lavalley JM (2025) Incorporating aridity in soil carbon steward-
1736 ship frameworks. *Nature Climate Change* 15(3):240–242. [https://doi.org/10.1038/](https://doi.org/10.1038/s41558-025-02270-9)
1737 [s41558-025-02270-9](https://doi.org/10.1038/s41558-025-02270-9)
1738
1739 Davidson EA, Samanta S, Caramori SS, et al (2012) The $\frac{1}{2}D_i$ and $\frac{1}{2}A_i$ Arrhenius and $\frac{1}{2}M_i$ Michaelis–Menten kinetics model for decom-
1740 position of soil organic matter at hourly to seasonal time scales. *Global Change*
1741 *Biology* 18(1):371–384. <https://doi.org/10.1111/j.1365-2486.2011.02546.x>
1742
1743 Dolui M, Nel T, Chacon S, et al (2026a) Soil Organic Matter Stabilization by
1744 Polyvalent Cations in a Buried Alkaline Soil. *Journal of Geophysical Research: Biogeosciences* 131(2). <https://doi.org/10.1029/2025JG009241>
1745
1746
1747
1748

Dolui M, Nel T, Phillips LM, et al (2026b) Composition and persistence of soil organic matter along eroding and depositional transects in buried vs. modern soil layers: A case of the Brady paleosol at Wauneta, Nebraska. <i>Geoderma</i> 465:117660. https://doi.org/10.1016/j.geoderma.2025.117660	1749 1750 1751 1752 1753
Elzhov T, Mullen K, Spiess A, et al (2023) minpack.lm: R Interface to the Levenberg-Marquardt Nonlinear Least-Squares Algorithm Found in MINPACK, Plus Support for Bounds. URL https://CRAN.R-project.org/package=minpack.lm .	1754 1755 1756 1757
Fierer N, Schimel JP (2003) A Proposed Mechanism for the Pulse in Carbon Dioxide Production Commonly Observed Following the Rapid Rewetting of a Dry Soil. <i>Soil Science Society of America Journal</i> 67(3):798. https://doi.org/10.2136/sssaj2003.0798	1758 1759 1760 1761 1762
Fontaine S, Barot S, Barré P, et al (2007) Stability of organic carbon in deep soil layers controlled by fresh carbon supply. <i>Nature</i> 450(7167):277–280. https://doi.org/10.1038/nature06275	1763 1764 1765 1766
Gao X, Huang R, Li J, et al (2020) Temperature induces soil organic carbon mineralization in urban park green spaces, Chengdu, southwestern China: Effects of planting years and vegetation types. <i>Urban Forestry & Urban Greening</i> 54:126761. https://doi.org/10.1016/j.ufug.2020.126761	1767 1768 1769 1770
Ghezzehei TA, Sulman B, Arnold CL, et al (2019) On the role of soil water retention characteristic on aerobic microbial respiration. <i>Biogeosciences</i> 16(6):1187–1209. https://doi.org/10.5194/bg-16-1187-2019	1771 1772 1773 1774
Goebel MO, Bachmann J, Woche SK, et al (2005) Soil wettability, aggregate stability, and the decomposition of soil organic matter. <i>Geoderma</i> 128(1-2):80–93. https://doi.org/10.1016/j.geoderma.2004.12.016	1775 1776 1777 1778
Griffiths BS, Philippot L (2013) Insights into the resistance and resilience of the soil microbial community. <i>FEMS Microbiology Reviews</i> 37(2):112–129. https://doi.org/10.1111/j.1574-6976.2012.00343.x	1779 1780 1781 1782
Hicks Pries CE, Castanha C, Porras RC, et al (2017) The whole-soil carbon flux in response to warming. <i>Science</i> 355(6332):1420–1423. https://doi.org/10.1126/science.aal1319	1783 1784 1785 1786
Hicks Pries CE, Ryals R, Zhu B, et al (2023) The Deep Soil Organic Carbon Response to Global Change. <i>Annual Review of Ecology, Evolution, and Systematics</i> 54(1):375–401. https://doi.org/10.1146/annurev-ecolsys-102320-085332	1787 1788 1789 1790
Hill RL, Horton R, Cruse RM (1985) Tillage Effects on Soil Water Retention and Pore Size Distribution of Two Mollisols. <i>Soil Science Society of America Journal</i> 49(5):1264–1270. https://doi.org/10.2136/sssaj1985.03615995004900050039x	1791 1792 1793 1794

- 1795 Horne D, McIntosh J (2000) Hydrophobic compounds in sands in New
1796 Zealand—extraction, characterisation and proposed mechanisms for repel-
1797 lency expression. *Journal of Hydrology* 231-232:35–46. [https://doi.org/10.1016/
1798 S0022-1694\(00\)00181-5](https://doi.org/10.1016/S0022-1694(00)00181-5)
- 1799
1800 Hunter BD, Roering JJ, Silva LCR, et al (2024) Geomorphic controls on the abun-
1801 dance and persistence of soil organic carbon pools in erosional landscapes. *Nature
1802 Geoscience* 17(2):151–157. <https://doi.org/10.1038/s41561-023-01365-2>
- 1803
1804 IPCC (2018) Global Warming of 1.5°C. In: Masson-Delmotte V, Zhai P, Pörtner HO,
1805 et al (eds) An IPCC Special Report on the impacts of global warming of 1.5°C
1806 above pre-industrial levels and related global greenhouse gas emission pathways, in
1807 the context of strengthening the global response to the threat of climate change.
1808 Intergovernmental Panel on Climate Change., <https://doi.org/10.1038/291285a0>
- 1809
1810 Jacobs PM, Mason JA (2004) Paleopedology of soils in thick Holocene loess, Nebraska,
1811 USA. *Revista Mexicana de Ciencias Geológicas* 21(1):54–70
- 1812
1813 Jacobs PM, Mason JA (2007) Late Quaternary climate change, loess sedimentation,
1814 and soil profile development in the central Great Plains: A pedosedimentary model.
1815 *Geological Society of America Bulletin* 119(3-4):462–475. [https://doi.org/10.1130/
1816 B25868.1](https://doi.org/10.1130/B25868.1)
- 1817
1818 Jobbagy EG, Jackson RB (2000) The Vertical Distribution of Soil Organic Carbon
1819 and Its Relation to Climate and Vegetation. *Ecological Applications* 10(2):423–436
- 1820
1821 Johnson WC, Willey KL (2000) Isotopic and rock magnetic expression of environ-
1822 mental change at the Pleistocene–Holocene transition in the central Great Plains.
1823 *Quaternary International* 67(1):89–106. [https://doi.org/10.1016/S1040-6182\(00\)
1824 00011-2](https://doi.org/10.1016/S1040-6182(00)00011-2)
- 1825
1826 Johnson WC, Willey KL, Mason JA, et al (2007) Stratigraphy and environmental
1827 reconstruction at the middle Wisconsinan Gilman Canyon formation type locality,
1828 Buzzard’s Roost, southwestern Nebraska, USA. *Quaternary Research* 67(3):474–
1829 486. <https://doi.org/10.1016/j.yqres.2007.01.011>
- 1830
1831 Kaiser M, Kleber M, Berhe AA (2015) How air-drying and rewetting modify soil
1832 organic matter characteristics: An assessment to improve data interpretation and
1833 inference. *Soil Biology and Biochemistry* 80:324–340. [https://doi.org/10.1016/j.
1834 soilbio.2014.10.018](https://doi.org/10.1016/j.soilbio.2014.10.018)
- 1835
1836 Kang S, Xing B (2008) Humic Acid Fractionation upon Sequential Adsorption onto
1837 Goethite. *Langmuir* 24(6):2525–2531. <https://doi.org/10.1021/la702914q>
- 1838
1839 Kemper WD, Rosenau RC, Dexter AR (1987) Cohesion Development in Disrupted
1840 Soils as Affected by Clay and Organic Matter Content and Temperature. *Soil Sci-
ence Society of America Journal* 51(4):860–867. <https://doi.org/10.2136/sssaj1987>.

03615995005100040004x 1841

Lawrence CR, Harden JW, Xu X, et al (2015) Long-term controls on soil organic carbon with depth and time: A case study from the Cowlitz River Chronosequence, WA USA. *Geoderma* 247-248:73–87. <https://doi.org/10.1016/j.geoderma.2015.02.005> 1842
1843
1844
1845
1846

Lawrence CR, Schulz MS, Masiello CA, et al (2021) The trajectory of soil development and its relationship to soil carbon dynamics. *Geoderma* 403:115378. <https://doi.org/10.1016/j.geoderma.2021.115378> 1847
1848
1849
1850

Leizeaga A, Hicks LC, Manoharan L, et al (2021) Drought legacy affects microbial community trait distributions related to moisture along a savannah grassland precipitation gradient. *Journal of Ecology* 109(9):3195–3210. <https://doi.org/10.1111/1365-2745.13550> 1851
1852
1853
1854
1855

Lenth RV (2024) emmeans: Estimated Marginal Means, aka Least-Squares Means. URL <https://CRAN.R-project.org/package=emmeans> 1856
1857
1858

Li Q, Hu W, Li L, et al (2023) Interactions between organic matter and Fe oxides at soil micro-interfaces: Quantification, associations, and influencing factors. *Science of The Total Environment* 855:158710. <https://doi.org/10.1016/j.scitotenv.2022.158710> 1859
1860
1861
1862

Liu T, Wang L, Feng X, et al (2018) Comparing soil carbon loss through respiration and leaching under extreme precipitation events in arid and semiarid grasslands. *Biogeosciences* 15(5):1627–1641. <https://doi.org/10.5194/bg-15-1627-2018> 1863
1864
1865
1866

Marin-Spiotta E, Chadwick OA, Kramer M, et al (2011) Carbon delivery to deep mineral horizons in Hawaiian rain forest soils. *Journal of Geophysical Research* 116(G3):G03011. <https://doi.org/10.1029/2010JG001587> 1867
1868
1869
1870

Marin-Spiotta E, Chaopricha NT, Plante AF, et al (2014) Long-term stabilization of deep soil carbon by fire and burial during early Holocene climate change. *Nature Geoscience* 7(6):428–432. <https://doi.org/10.1038/ngeo2169> 1871
1872
1873
1874

Mason JA, Jacobs PM, Hanson PR, et al (2003) Sources and paleoclimatic significance of Holocene Bignell Loess, central Great Plains, USA. *Quaternary Research* 60(3):330–339. <https://doi.org/10.1016/j.yqres.2003.07.005> 1875
1876
1877
1878

Mason JA, Miao X, Hanson PR, et al (2008) Loess record of the Pleistocene–Holocene transition on the northern and central Great Plains, USA. *Quaternary Science Reviews* 27(17-18):1772–1783. <https://doi.org/10.1016/j.quascirev.2008.07.004> 1879
1880
1881
1882

McDowell T (2020) Processes controlling soil hydrology and pedogenic carbonate formation in loess tablelands, Nebraska, USA. PhD thesis, University of Wisconsin-Madison, Madison 1883
1884
1885
1886

- 1887 McDowell TM, Mason JA, Vo T, et al (2022) Hydrology of a Semiarid Loess-Paleosol
1888 Sequence, and Implications for Buried Soil Connection to the Modern Climate,
1889 Plant-Available Moisture, and Loess Tableland Persistence. *Journal of Geophysical*
1890 *Research: Earth Surface* 127(12). <https://doi.org/10.1029/2022JF006800>
1891
- 1892 McMurtry AR, Kasmerchak CS, Vaughan EA, et al (2024) Getting to the root of
1893 the problem: Soil carbon and microbial responses to root inputs within a buried
1894 paleosol along an eroding hillslope in southwestern Nebraska, USA. *Soil Biology and*
1895 *Biochemistry* 198:109549. <https://doi.org/10.1016/j.soilbio.2024.109549>
1896
- 1897 Miao X, Mason JA, Swinehart JB, et al (2007) A 10,000 year record of dune activity,
1898 dust storms, and severe drought in the central Great Plains. *Geology* 35(2):119.
1899 <https://doi.org/10.1130/G23133A.1>
- 1900 Miller A, Schimel J, Meixner T, et al (2005) Episodic rewetting enhances carbon and
1901 nitrogen release from chaparral soils. *Soil Biology and Biochemistry* 37(12):2195–
1902 2204. <https://doi.org/10.1016/j.soilbio.2005.03.021>
1903
- 1904 Min K, Berhe AA, Khoi CM, et al (2020) Differential effects of wetting and drying on
1905 soil CO₂ concentration and flux in near-surface vs. deep soil layers. *Biogeochemistry*
1906 148(3):255–269. <https://doi.org/10.1007/s10533-020-00658-7>
1907
- 1908 Najera F, Dippold MA, Boy J, et al (2020) Effects of drying/rewetting on soil aggregate
1909 dynamics and implications for organic matter turnover. *Biology and Fertility of Soils*
1910 56(7):893–905. <https://doi.org/10.1007/s00374-020-01469-6>
1911
- 1912 Naorem A, Jayaraman S, Dalal RC, et al (2022) Soil Inorganic Carbon as a Potential
1913 Sink in Carbon Storage in Dryland Soils—A Review. *Agriculture* 12(8):1256. <https://doi.org/10.3390/agriculture12081256>
1914
- 1915
- 1916 Neff JC, Asner GP (2001) Dissolved Organic Carbon in Terrestrial Ecosystems: Syn-
1917 thesis and a Model. *Ecosystems* 4(1):29–48. <https://doi.org/10.1007/s100210000058>
1918
- 1919 Or D, Tuller M (1999) Liquid retention and interfacial area in variably saturated
1920 porous media: Upscaling from single-pore to sample-scale model. *Water Resources*
1921 *Research* 35(12):3591–3605. <https://doi.org/10.1029/1999WR900262>
1922
- 1923 Pal SC, Chakraborty R, Towfiqul Islam ARM, et al (2023) Land use and climate
1924 change-induced soil erosion mapping in a sub-tropical environment. *Geomatics,*
1925 *Natural Hazards and Risk* 14(1). <https://doi.org/10.1080/19475705.2023.2270129>
- 1926 Patton NR, Lohse KA, Seyfried MS, et al (2019) Topographic controls of soil organic
1927 carbon on soil-mantled landscapes. *Scientific Reports* 9(1):6390. <https://doi.org/10.1038/s41598-019-42556-5>
1928
- 1929
- 1930 Pausch J, Loeppmann S, Kühnel A, et al (2016) Rhizosphere priming of barley with
1931 and without root hairs. *Soil Biology and Biochemistry* 100:74–82. <https://doi.org/>
1932

10.1016/j.soilbio.2016.05.009 1933

Pinheiro J, Bates D, DebRoy S, et al (2024) nlme: Linear and Nonlinear Mixed Effects Models. URL <https://CRAN.R-project.org/package=nlme> 1934

R Core Team (2025) R: A Language and Environment for Statistical Computing. URL <https://www.r-project.org/> 1935

Rasmussen C, Heckman K, Wieder WR, et al (2018) Beyond clay: towards an improved set of variables for predicting soil organic matter content. *Biogeochemistry* 137(3):297–306. <https://doi.org/10.1007/s10533-018-0424-3> 1936

RStudio Team (2019) RStudio: Integrated Development for R. RStudio. URL <http://www.rstudio.com/> 1937

Rumpel C, Kögel-Knabner I (2011) Deep soil organic matter—a key but poorly understood component of terrestrial C cycle. *Plant and Soil* 338(1-2):143–158. <https://doi.org/10.1007/s11104-010-0391-5> 1938

Schmidt MWI, Torn MS, Abiven S, et al (2011) Persistence of soil organic matter as an ecosystem property. *Nature* 478(7367):49–56. <https://doi.org/10.1038/nature10386> 1939

Schrumpf M, Kaiser K, Guggenberger G, et al (2013) Storage and stability of organic carbon in soils as related to depth, occlusion within aggregates, and attachment to minerals. *Biogeosciences* 10(3):1675–1691. <https://doi.org/10.5194/bg-10-1675-2013> 1940

Shariffar A, Minasny B, Arrouays D, et al (2023) Soil inorganic carbon, the other and equally important soil carbon pool: Distribution, controlling factors, and the impact of climate change. p 165–231, <https://doi.org/10.1016/bs.agron.2022.11.005> 1941

Six J, Conant R, Paul E, et al (2002) Review: Stabilization Mechanisms of Soil Organic Matter: Implications for C-Saturation of Soils. *Plant and Soil* 241(2):155–176 1942

Slessarev EW, Chadwick OA, Sokol NW, et al (2022) Rock weathering controls the potential for soil carbon storage at a continental scale. *Biogeochemistry* 157(1):1–13. <https://doi.org/10.1007/s10533-021-00859-8> 1943

Soong JL, Castanha C, Hicks Pries CE, et al (2021) Five years of whole-soil warming led to loss of subsoil carbon stocks and increased CO₂ efflux. *Science Advances* 7(21). <https://doi.org/10.1126/sciadv.abd1343> 1944

Stacy EM, Hart SC, Hunsaker CT, et al (2015) Soil carbon and nitrogen erosion in forested catchments: implications for erosion-induced terrestrial carbon sequestration. *Biogeosciences* 12(16):4861–4874. <https://doi.org/10.5194/bg-12-4861-2015> 1945

Steenwerth K, Jackson L, Calderon F, et al (2005) Response of microbial community composition and activity in agricultural and grassland soils after a simulated rainfall. 1946

1979 Soil Biology and Biochemistry 37(12):2249–2262. <https://doi.org/10.1016/j.soilbio.2005.02.038>

1980

1981

1982 Szymanski LM (2021) Spatial Distribution and Long-Term Persistence of Ancient

1983 Carbon in Buried Soils and Its Vulnerability to Landscape Disturbance. PhD thesis,

1984 University of Wisconsin-Madison, Madison

1985

1986 Thaler EA, Larsen IJ, Yu Q (2021) The extent of soil loss across the US Corn Belt.

1987 Proceedings of the National Academy of Sciences 118(8). [https://doi.org/10.1073/](https://doi.org/10.1073/pnas.1922375118)

1988 [pnas.1922375118](https://doi.org/10.1073/pnas.1922375118)

1989

1990 Tsypin M, Macpherson G (2012) The effect of precipitation events on inor-

1991 ganic carbon in soil and shallow groundwater, Konza Prairie LTER Site, NE

1992 Kansas, USA. Applied Geochemistry 27(12):2356–2369. [https://doi.org/10.1016/j.](https://doi.org/10.1016/j.apgeochem.2012.07.008)

1993 [apgeochem.2012.07.008](https://doi.org/10.1016/j.apgeochem.2012.07.008)

1994 Venables WN, Ripley BD (2002) MASS (Modern Applied Statistics with S). URL

1995 <https://CRAN.R-project.org/package=MASS>

1996

1997 Wahab LM, Kim S, Berhe AA (2025) Carbon and Nitrogen Dynamics in Subsoils

1998 After 20 years of Added Precipitation in a Mediterranean Grassland. [https://doi.](https://doi.org/10.5194/egusphere-2024-3607)

1999 [org/10.5194/egusphere-2024-3607](https://doi.org/10.5194/egusphere-2024-3607)

2000

2001 Xiang SR, Doyle A, Holden PA, et al (2008) Drying and rewetting effects on C and

2002 N mineralization and microbial activity in surface and subsurface California grass-

2003 land soils. Soil Biology and Biochemistry 40(9):2281–2289. [https://doi.org/10.1016/](https://doi.org/10.1016/j.soilbio.2008.05.004)

2004 [j.soilbio.2008.05.004](https://doi.org/10.1016/j.soilbio.2008.05.004)

2005

2006 Yoo K, Amundson R, Heimsath AM, et al (2006) Spatial patterns of soil organic

2007 carbon on hillslopes: Integrating geomorphic processes and the biological C cycle.

2008 Geoderma 130(1-2):47–65. <https://doi.org/10.1016/j.geoderma.2005.01.008>

2009

2010 Zhu B, Cheng W (2013) Impacts of drying–wetting cycles on rhizosphere respiration

2011 and soil organic matter decomposition. Soil Biology and Biochemistry 63:89–96.

2012 <https://doi.org/10.1016/j.soilbio.2013.03.027>

2013

2014

2015

2016

2017

2018

2019

2020

2021

2022

2023

2024